IZMIR DEMOCRACY UNIVERSITY

NATURAL & APPLIED SCIENCES JOURNAL

IDUNAS

E-ISSN: 2645-9000

Year: 2021

Volume: 4, Issue: 2

Table of Contents

DOI: 10.38061/idunas.850545

IDUNAS	NATURAL & APPLIED SCIENCES JOURNAL	2021 Vol. 4 No. 2 (1-15)

Machine Vision Supported Quality Control Applications in Rotary Switch Production by Using Both Process FMEA and Design FMEA

Research Article

İsmet Karacan[1*], İnanç Erdoğan[1*], M. Cem İğdil[1*], Ufuk Cebeci[2*]

[1]AN-EL Anahtar ve Elektrikli Ev Aletleri A.Ş., Velibaba Mah., Ankara Cad., No:188, Pendik, 34896, İstanbul/Türkiye.

[2] Industrial Engineering Department, İstanbul Technical University, İstanbul, Türkiye.

Author E-mails
anelprs142@an-el.com.tr
anel@an-el.com.tr
arge6@an-el.com.tr
cebeciu@itu.edu.tr
*Correspondance to: İsmet Karacan, AN-EL Anahtar ve Elektrikli Ev Aletleri A.Ş., Velibaba Mah., Ankara Cad., No:188, Pendik, 34896, İstanbul/Türkiye.
DOI: 10.38061/idunas.850545

Received: 30.12.2020; Accepted: 04.03.2021

Abstract

Emerging in the past few decades, Industry 4.0 has wide effects over production lines with an increasing number of novel applications. These applications implement more than one of the tools of Industry 4.0. These tools include but are not limited to internet of things (IoT), big data, cloud computing, artificial intelligence, augmented reality, virtual reality, machine to machine communication (M2M), smart robot applications, etc. The aim of these efforts is mainly to acquire smarter manufacturing systems. With spreading Industry 4.0 methodologies, the role of sensors became more important to respond to new demands. One of the most important sensor types in this sense is the camera which now has wide variants in different forms. Applying machine vision algorithms via cameras grants optimization of many critical processes. In this perspective, the quality of both product and process should be handled as a key performance indicator that may be continuously enhanced for excellence. Machine vision algorithms may be adapted to check and manage quality in designated control points on the production lines. This study focuses on the control of the quality of rotary switches that are widely used in household appliances like ovens and washing machines. Rotary switches are critical components of an appliance since they direct the flow of electricity within the product. A failure in the functionality of this component directly causes the failure of the main product. Hence, the quality rate of rotary switches should be calculated in defective parts per million (dppm) units. An intense quality control procedure is required to achieve low dppm rates during production. As a real-life application, a camera system is integrated into the rotary switch production line on a selected point. Classification algorithms are developed on a cost-effective platform to perform visual quality checks of the rotary switches and qualify as “Ok” or “Defective”. The selected point ensures a high percent check of quality criteria while enabling repair of the defective parts with minor interventions. This control aims to identify a defective rotary switch as soon as possible since most of the defects are irreversible

once the rotary switch is totally produced or even some processes are completed. In this case, the entire product should be set apart for scrap.
Another originality of our study is applying both Process Failure Mode and Effect Analysis (PFMEA) and Design Failure Mode and Effect Analysis (DFMEA) together. There is almost no referenced study in the literature.
Benchmark comparisons are conducted upon completing the integration of the new system to the production line. As a result, enhancements in the quality, cost, and production speed parameters are achieved with a cost-effective smart system. Additional capabilities are added to the system, namely data analyzing online data feeding.
Keywords: Machine vision, Industry 4.0, Quality Control, FMEA, Poka-Yoke

1. INTRODUCTION

With rapidly developing technologies, consumer behavior has been exposed to changes concerning purchasing habits. The simplicity of the e-Commerce experience has especially increased the number of criteria that are considered during the selection of a product or a service [1]. With this change, manufacturers also updated their strategies to manage customer demand to enable them to compete in the market. For instance, agile manufacturing is a newly emerging methodology that is based on adding value to the customer with short-term and high-frequency sprints [2]. One of the key criteria considered is the customer's perception of the brand on quality. Many firms spend their years increasing their loyalty by releasing high-quality end products. One of the aspects of this success is improving the quality control capabilities during the production process. Many soft and hard tools have been developed to ensure that products are manufactured within defined quality limits. Statistical Process Control, histograms, Poka-Yoke devices are widely used examples of control tools.

Global technological developments force producers to perpetually enhance their key operational skills. Industrial revolutions have been providing key guidance for these technology-driven steps. The up-to-date concept of Industry 4.0 is mainly based on data and knowledge-related tools. Recent advances in sensors and computational power encourage developers to implement novel applications developed with complex algorithms. Machine vision-supported classification algorithms are widely used to have more robust quality inspections to avoid defective parts during the process.

A rotary switch is an electrical component with multiple positions that provides the requested terminal sequence in accordance with the corresponding function diagram. Rotary switches are widely used for the manufacturing of household appliances like ovens and washing machines. Accoupled with a control knob, rotary switches shift the electrical functioning state of the appliance once the knob is rotated by the user. Hence, rotary switches are critical elements that directly affect the performance of the appliance. As a result, intensive care should be spent during the production phase of switches to avoid any functional defect.

In this study, we describe a low-cost machine vision Poka-Yoke (Mistake Proofing) application that is empowered by a Decision Tree Classifier algorithm to detect defective parts during the rotary switch production process. The hardware consists of a Raspberry Pi-based computing system, touch panel for operators, camera, lighting, and custom interface PCB for the connection to the production system. OpenCV library is deployed to handle machine vision operations and classification algorithms are coded in Python language. The distinguishing approach of this study is the utilization of FMEA methods. This application is assessed by both PFMEA and DFMEA during the development phase. To the best of the authors' knowledge, this is the first study that integrates PFMEA and DFMEA in a visual quality control application. Section 2 includes a literature review of similar applications. Section 3 describes the proposed methodology. The results are shared in Section 4. Final remarks and conclusions are included in Section 5.

2. LITERATURE REVIEW

Machine Vision Supported Quality Control

For the sake of rapidly improving technology, Commercial off-the-shelf (COTS) products are widely preferred to include in cost-effective optimization solutions. One of these fields is the optical process and quality control during production. This study suggests a Raspberry Pi-based application for quality control on a production line. Similar approaches exist in the literature for production lines. Louw and Droomer [3] proposed a Raspberry Pi-based hardware system to defects on toy trains in which OpenCV has been implemented for machine vision operations and Python has been selected for coding statistical classifiers. Würschinger et al. [4] applied Convolutional Neural Networks (CNN) algorithm on Raspberry Pi to suggest an enhanced and low-cost deep learning solution for manufacturing lines where they try to detect chips on piston rods via a deep learning algorithm with two classes. In another application by Ardhy and Hariadi [5], Raspberry Pi, Python, and OpenCV integration has been utilized to inspect Printed Circuit Board (PCB) defects and authors suggested Adaptive Gaussian Threshold as the best defect identifier. The study for welding visual inspection by Gong et al. [6] also suggests a low-cost system where they inspect the quality of welding on circuits via a Support Vector Machine Algorithm. Korodi et al. [7] deploy another low-cost visual system to control quality Electronic Control Unit (ECU) control in the automotive industry. The proposed system checks the missing or defective pins, clips, cracks on electronic boards, etc. with the help of a visual control system. Merging the data by a parallel acquisition and parallel processing the information methodology, they provide a robust defect detection system where the produced components are safety-critical. Adamo et al. [8] joined several CMOS cameras to acquire the image of satin glass in production lines. The acquired image was processed via the Canny edge detection algorithm. Frustaci et al. [9] suggested another embedded machine vision system for geometric inspection for planar or rotational shifts on the product in the context of Industry 4.0. The target product for quality control is the catalytic converter on which they applied image processing steps as image acquisition, conversion from RGB to grayscale, Region of interest (ROI) filtering for removing noise, Canny edge detection algorithm, Contour selection, Morphological filtering, and Center detection. Without having integrated to production lines, Parakontan and Sawangsri [10] designed another Raspberry-Pi-based system to control the quality of printed circuit boards (PCB) against copper leakages by transforming RGB images to binary images. Leo et al. [11] developed a two-camera vision system to detect multiple types of defects about dimensions and shapes on electromechanics part production and integrated the system into the production line. The proposed architecture of the study includes the integration of two cameras to a Programmable logic controller (PLC) via an industrial PC where data acquisition algorithms run. The system was managed by Labview software. Moru and Borro [12] developed a custom application on Machine Vision to control dimensions of produced gears on production lines. To avoid measuring errors as much as possible and provide enhanced tolerances, their proposed system includes the acquisition of the image with telecentric lenses and intense calibration operations. Another contribution of their study is the methodological approach for determining uncertainty associated with their proposed measurement process.

Revealing the literature shows that many studies have been proposed with different configurations according to the application area, size of the project, demand for computational power, the budget of the project, integrability to the production line, etc. Many requirements could be met by Raspberry Pi-based low-cost systems, where a moderate hardware performance with an open-source image processing/classification algorithm may provide the necessary performance. For more demanding computations like deep learning or integration requirements, a common combination is the integration of industrial cameras to PLCs via industrial PCs. Independent from the hardware, OpenCV is the most widespread image processing software that is applied for image acquisition and processing purposes like binarization, converting, filtering, etc. in these projects. The current trend of studies advises that machine

vision applications will drastically increase to be integrated into automated systems where intense quality control activities are required.

Decision Tree Classifier (DTC)

Classification methodology is the systematic process of categorizing entities according to the defined criteria. A Decision Tree Classifier stays among many alternatives of multistage classifiers [13]. The process is used to predict a target variable [14]. The target variable may be continuous or categorical. The method has many applications in production systems. Wang et al. suggested a new approach that can identify patterns of control charts [15]. Matsko et al. proposed an adaptive fuzzy classifier that has a dynamic structure that can be adapted to control Automatic Process Control Systems [16]. Putri et al. prepared a decision tree that reflects the methodology of identifying defects on a grinding wheel [17].

Integration of Visual Quality Control and Decision Tree Classifiers are also common in production. Cheng et al. implemented an online machine vision-supported decision tree algorithm to ease the decision-making process of combine harvesters on impurities of rice grain [18]. Zhou et al. suggested another machine vision system that can detect surface defects of automobiles during their production [19]. Lin et al. developed a machine vision-supported decision tree classifier that can reveal defects of optic lenses in their manufacturing phase [20]. There are many different examples in the literature for various types of productions since the methodology can manage to identify many types of "defects". In this study, the Classification and Regression Trees (CART) classification algorithm which was proposed by Breiman et al. [21] preferred since the algorithm is appropriate to manage binary or categorical parameters and variables.

Failure Mode and Effect Analysis (FMEA)

With a wide definition, FMEA is a systematic approach to evaluate a process, system, design, or service to explore in which way failures can occur [22]. The method may be applied to reveal shortcomings of an ongoing process or risks on a design of a product in the development phase. The method has originated in a Military Procedure of the United States Department of Defense with some shortcomings [23]. It has been widely applied to many National Aeronautics and Space Administration (NASA) space programs [24]. Today, FMEA has many applications in manufacturing industries. It is among the most powerful tools to determine the lack of a product design or production process. Maddalena et al. applied DFMEA in the feasibility phase of Automotive CMOS Image Sensors development [25]. Klochkov et al. assessed the process of can stock production by a detailed PFMEA [26]. Since there are numerous studies, many literature review papers can be encountered in the literature. Sharma and Srivastava surveyed FMEA methods with a scope basis and included many studies and their contributions [27]. Spreafico et al have introduced a state-of-the-art survey of 220 papers and supported the review with 109 relevant patent information [28]. Huang et al. represented a systematic literature review and gave insights regarding the future of FMEA [29]. Ng et al. provided information on a more capable deployment of FMEA by integrating to other tools such as inventive problem-solving methodology (TRIZ), Quality Function Deployment (QFD), and Root Cause Analysis (RCA) [30].

Combining our literature review on Machine Vision-based Quality control and FMEA discloses that there is a lack of integrating DFMEA and PFMEA at the application level. According to our research, we have not found any research about combining PFMEA and DFMEA. DFMEA reflects the risks on the product design where PFMEA helps to manage risks on the manufacturing of a product. As a contribution of this study, combining both FMEAs provides a more robust insight to determine the most critical risks on the quality of the produced product since the combination contains both risks that can be met on product and risks that can be occurred during the production of the product. Another originality is the representation of both DFMEA and PFMEA in a common FMEA table.

3. PROPOSED METHODOLOGY

The firm AN-EL A.S. is an electromechanics component producer for household appliances in Turkey. Rotary Switch in Figure 1 is a wide product family which is manufactured by AN-EL A.S. and sold to household appliance producers especially to be assembled to cooking devices. Since the firm exports 85 percent of products to worldwide plants, especially to global production sites, the quality of the final product has utmost importance for a sustainable commercial relationship.

Figure 1. Rotary Switch (Bottom View)

Table 1. Severity, Probability, and Detectability Criteria

Rank	Severity	Probability	Detectability
10	May endanger machine or assembly operator. Very high severity ranking when a potential failure mode affects safe product operation and/or involves noncompliance with regulations without a warning.	≥ 100 per thousand (1,000) pieces ≥ 1 in 10	Absolute certainty of non-detection.
9	May endanger machine or assembly operator. Very high severity ranking when a potential failure mode affects safe product operation and/or involves noncompliance with regulations with a warning.	50 per thousand (1.000) pieces 1 in 20	Controls will probably not detect.
8	Major disruption to the production line. Product/item inoperable (loss of primary function). 100 % of products should be scrapped.	20 per thousand (1.000) pieces 1 in 50	Controls may seldomly detect.
7	Minor disruption to the production line. Product/item operable but at a reduced level of performance. Customer very dissatisfied. A high portion of the product should be scrapped.	10 per thousand (1.000) pieces 1 in 100	Controls have a poor chance of detection.
6	Minor disruption to the production line. Product/item operable but Convenience/Feature item(s) inoperable. Customer dissatisfied. A low portion of the product should be scrapped.	2 per thousand (1.000) pieces 1 in 500	Controls may detect case by case.
5	Minor disruption to the production line. Product/item operable but Convenience/Feature item(s) operable at a reduced level of performance. The product should be sorted and reworked.	1 per thousand (1.000) pieces 1 in 1.000	Controls may detect.
4	Minor disruption to the production line. Fit and Finish/Squeak and Rattle item does not conform. Defect noticed by most customers (greater than 75%). The product should be sorted, and a high portion should be reworked.	0.5 per thousand (1.000) pieces 1 in 2.000	Controls may have a good chance to detect.
3	Minor disruption to the production line. Fit and Finish/Squeak and Rattle item does not conform. Defect noticed by 50% of customers. The product should be sorted, and a moderate portion should be reworked.	0.1 per thousand (1.000) pieces 1 in 10.000	Controls have a good chance to detect.
2	Minor disruption to the production line. Fit and Finish/Squeak and Rattle item does not conform. Defect noticed by discriminating customers (less than 25%). The product should be sorted, and a low portion should be reworked.	≤ 0.1 per thousand (1.000) pieces	Controls almost certain to detect.

1	No effect.	Failure is eliminated through preventative control	Controls certain to detect.

The rotary switch can be produced by assembling multiple semi-products in a production line. Most of the parts are sensitive to external factors such as humidity and pressure. Hence, an intense production process is required to acquire precise final products. Such a process requires continuous improvement actions to assure a high level of quality. An appropriate way to ensure this quality is periodically analyzing the product and production process with analytical tools.

Table 2. PFMEA for Rotary Switch Production

Process Step	Failure Mode	Failure Effect	Sev.	Prob.	Det.	RPN	Prevention/Action
Assembly of Moving Terminals by Press	Wrong Sequence	Wrong functionality, should be scrapped	9	5	4	180	- Increasing the number of workers for control - A Poka-Yoke Device that checks the sequence electrically. - A Machine Vision supported Poka-Yoke device
Assembly of Moving Terminals by Press	Wrong types of moving terminal	Wrong functionality, should be scrapped	9	5	3	135	- Increasing the number of workers for control - A Poka-Yoke Device that checks the sequence electrically. - A Machine Vision supported Poka-Yoke device
Assembly of Fixed Terminals by Press	Wrong types of fixed terminal	Wrong functionality, should be scrapped	6	5	3	90	- Increasing the number of workers for control - A Poka-Yoke Device that checks the sequence electrically. - A Machine Vision supported Poka-Yoke device
Pressing Fixed Terminals	Missing Number of Fixed Terminals	Wrong functionality, should be reworked	7	4	3	84	- Can be checked visually before pressing - A Machine Vision supported Poka-Yoke device - Missing terminals should be pressed
Camshaft integration	Use of the wrong camshaft	Wrong functionality, should be reworked	7	3	3	63	- Can be checked visually before pressing - A Poka-Yoke Device for functionality test - Eliminating different types of the camshaft from the feeder with an additional process - Camshaft should be reassembled.
Nut assembly	Mis-assembly of nuts to body	Switch cannot be assembled to main appliance	5	4	3	60	-Can be checked by the operator. - A Poka-Yoke device for alignment.
Press of Fixed Terminals	Low pressing pressure	Loose terminals, risk of removal	6	3	3	54	- Can be checked with a pneumatic device - Terminals should be pressed again.
Protective Cover Assembly	Missing Cover	Moving terminals may be harmed	7	3	2	42	- Visual control by the operator - Machine vision supported Poka-Yoke device

Assembly of Spring	Wrong spring selection	Rotation torque may differ	4	3	3	36	-Can be checked with a Torque meter. - A Poka-Yoke device with torque measurement capability.
D Profile Assembly	Unoriented D Profile angle	Bad visual effect for final customer	4	3	3	36	- Can be checked visually by the operator. - A Poka-Yoke device with angle measurement capability.
Nut Assembly	Missing Nuts	Switch cannot be assembled to main appliance	5	2	2	20	-Can be checked by the operator. - A Poka-Yoke device for nut control.

One of the most important tools for these analyses is FMEA. The classical FMEA process with Severity, Probability, and Detectability criteria is applied to determine the most critical risks. Severity, Probability, and Detectability determining criteria for this study are shown in Table 1. The criteria in Table 1 have been prepared in line with the FMEA Handbook by Automotive Industry Action Group (AIAG) [31].

Upon identifying the scores of each risk, the Risk Priority Number (RPN) should be calculated with the formula in Equation 1 as the product of Severity, Probability, and Detectability [31]. An RPN value may change between 1 and 1.000 since Severity, Occurrence, and Detection may take values between 1 and 10.

$$RPN = Severity \times Occurrence \times Detection \quad (1)$$

Table 2 contains the risks of the production process by scoring their severity, probability, and detectability scores, failure mode, possible effect, and preventive actions. The PFMEA list has been sorted in descendant order concerning RPN values.

Table 3 indicates five items of DFMEA. The remarkable point for both DFMEA and PFMEA is having the risks for moving terminal on the top of the list. Since the FMEA items are recalculated in the Results section after integration of the proposed system, selected action and results are not included in Table 2 and Table 3.

Table 3. DFMEA for Rotary Switch Production

Related Part	Failure Mode	Failure Effect	Sev.	Prob.	Det.	RPN	Prevention/Action
Moving Terminal	Deformed moving terminal	Avoiding functionality, should be scrapped	8	4	5	160	- Increasing the number of workers for control - A Machine Vision supported Poka-Yoke device - A new selection process for deformed terminals
Switch Body	Soft housing for terminals	The terminal may be removed	8	3	3	72	- Change on pressing process - Mould modification - New raw material mixture for a harder body
Switch Body / Terminal	Incompatible tolerances	Inappropriate assembly of terminals	6	4	3	72	- Controlling product tolerances - Change of production process for more precise tolerances

D Profile Assembly	Size based assembly problem	Cannot assembly D Profile	5	3	4	60	- Update tolerances on mold - Use of cutters for reducing size on non-conforming D profiles.
All Plastics	Observation of burr	Visual	4	4	2	32	- Can be perceived as a quality problem by customers. - Burrs should be removed. - Update on mold design.

Moving terminals that are used for this production have various types as shown in Figure 2. According to DFMEA and PFMEA analysis, the quality requirements in concern of this study consist of the use of correct types, correct sequence, and correct assembly of moving terminals that don't have any deformation.

Figure 2. Various Types of Moving Terminals

Pareto Analysis has been completed by aggregating both PFMEA and DFMEA risks in descending order according to their RPN values and selecting the most critical risks in concern. Three out of 16 risks have been selected upon evaluation of the Pareto Chart in Figure 3 which have distinctly higher values compared to the remaining risks and are equal to nearly 20 percent (16 x 20 % = 3.2) of the total risks.

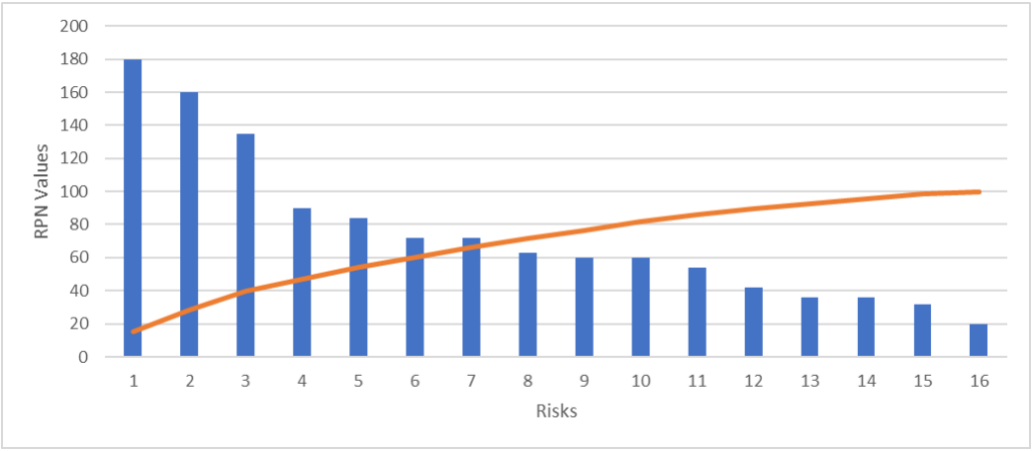

Figure 3. Pareto Analysis Chart of RPN Values of DFMEA and PFMEA

Selected risks that have a high impact on quality prove that the most critical items in the process are moving terminals. This conclusion is not surprising since moving terminals are assembled to the body of the rotary switch by an irreversible pressing operation. Moving terminals cannot be removed from the body after pressing, hence any failure results in a scrap of body and moving terminals. Moving terminals are the most expensive components among semi-products. Scrapping moving terminals and body sources a burdensome quality cost to the whole production.

Severity over 8 should be handled carefully. Since severity cannot be improved without design modification, a process enhancement is intended to improve probability and detectability values. The most common suggestion is to avoid risks with mistake-proofing (Poka-Yoke) [32]. The final decision to avoid any production risks has been determined as integrating a Poka-Yoke device into the production line. After evaluating several alternatives, the conclusion was developing a machine vision-supported Poka-Yoke Device. To achieve this quality control capability by machine vision, multiple low-cost alternatives are examined. Raspberry Pi-4 has been selected to provide sufficient computational power. Raspberry Pi-4 has been integrated into a touch screen as shown in Figure 4.

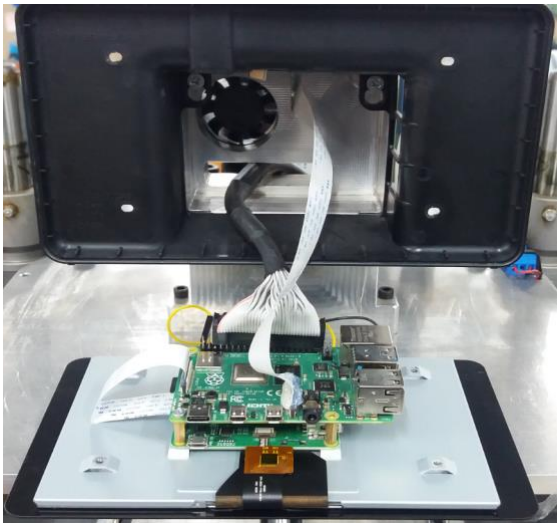

Figure 4. Inner Structure of the System

The configuration for the optical quality control system has been completed by adding lighting, camera, and interfaces. The resulting system is demonstrated in Figure 5. The new system is designed to be operated by a single operator. Additionally, the system can check two rotary switches simultaneously. Helping to increase the accuracy of the classification, it is also intended to decrease the processing time of the control since there has been detected a bottleneck for the process.

Figure 5. Integrated Quality Control System to Check Moving Terminals

Image operations of this process are conducted via OpenCV. A single switch has 9 circuit lines on its body. Analyzing the construction and alternatives of the combinations, it has been determined that 4 features for each line suffice to determine the type and the condition of the moving terminal. Additional 8 features between lines help to determine if a shunt exists between two adjacent lines. A total of 44 discrete lines on the rotary switches are checked during the image processing phase for robust classification. These lines are indicated in Figure 6 with blue color including their enumeration.

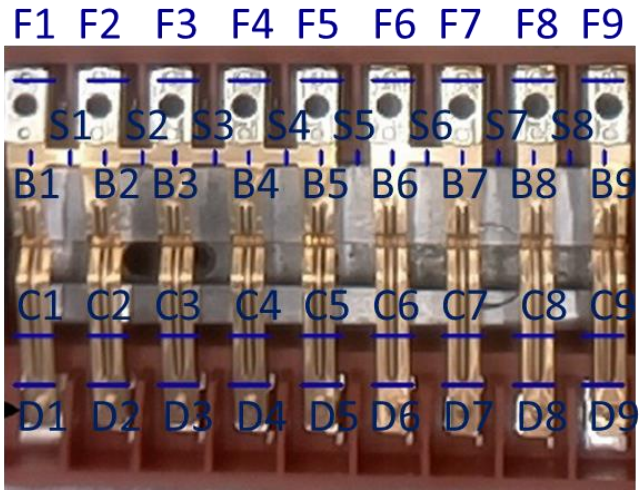

Figure 6. 44 Features on Rotary Switch for Classification

The feature points in Figure 6 are used to determine the type of the terminal and the connection between each terminal. Possible 6 types of terminal alternatives are shown in Figure 7. From left to right, the first line has a complete moving terminal with a fixed terminal on the opposite side, the second line has a semi terminal, the third line has a shunt that is used to connect to adjacent terminals, the fourth line has only a fixed terminal on the opposite side, the fifth line has a semi terminal that has a fixed terminal on the opposite side, and the sixth line has a shunt that has a fixed terminal on the opposite side.

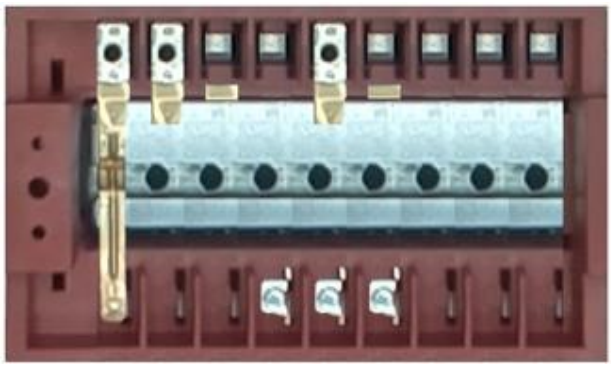

Figure 7. Types of the Possible Terminals

The types of terminals have been enumerated from 1 to 6 from left to right. If the line contains no terminals, the type is valued with 0. The connection between terminals is also considered to have the value 1 if there is a shunt between two adjacent terminals, 0 otherwise. Hence, a vector with size 9 can identify the terminals on the lines while a vector with size 8 can define the connections between terminals. The combined vector with 17 digits can define the connection type of a rotary switch.

The existence of metal parts can be detected and evaluated according to RGB values. The target variable for the classification algorithm is the connection vector with 44 digits which is converted according to the connection vector with 17 digits. The digit of the target variable is 0 if the feature should be metal

and 0 if otherwise. 9 digits of the connection vector can take the values from 0 to 7. The last 8 digits are binaries with 0 and 1. Hence the number of possible connection types is over 10 billion. Supplying the RGB values of 44 points to the classification algorithm enables it to determine the connection vector. The vector has been compared to the actual vector as training data. To achieve a smooth image processing process, a LED lighting has been mounted on the rotary switches in the line. Hence, a better contrast between plastic and metal parts can be acquired, since metal parts shine under lighting where plastic parts remain dark. 3.500 trials have been carried out to train classification algorithm on threshold values over which it is assessed that the underlying surface is metal with a smooth form. It has been also assured by lighting that the RGB values of deformed metal parts also remain below the threshold value. Most bright RGB value in feature lines has been selected for further evaluations on metal component existence. Figure 8 summarizes the overall process.

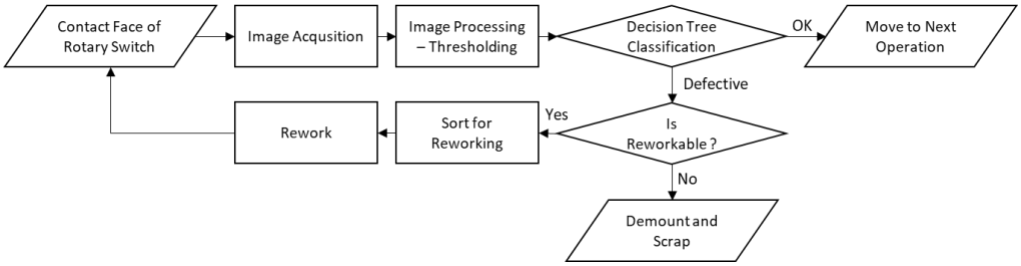

Figure 8. Machine Vision Supported Quality Control Process Flow

The classification algorithm suggests the threshold intervals for RGB values for each vector as in Table 4 where X is the clusters of numbers from 1 to 9 for F, B, C, and D, from 0 to for S.

Table 4. RGB Threshold values for Metal Detection

Vector\Component	Red	Green	Blue
FX	(140,255)	(110,255)	(110,255)
SX	(155,255)	(120,255)	(110,255)
BX	(155,255)	(120,255)	(110,255)
CX	(115,255)	(110,255)	(95,255)
DX	(150,255)	(130,255)	(130,255)

CART classification algorithm has been applied in this study since the algorithm is capable of handling binary parameters and variables. Providing RGB values of 44 features, the algorithm predicts the connection type of the rotary switch with a 17-digit vector. During the real production phase, The operator is informed about the prediction of the classification algorithm via touch screen as shown in Figure 9. For defective parts, additional information on defect points is highlighted with an enumeration to inform defective points on the rotary switch.

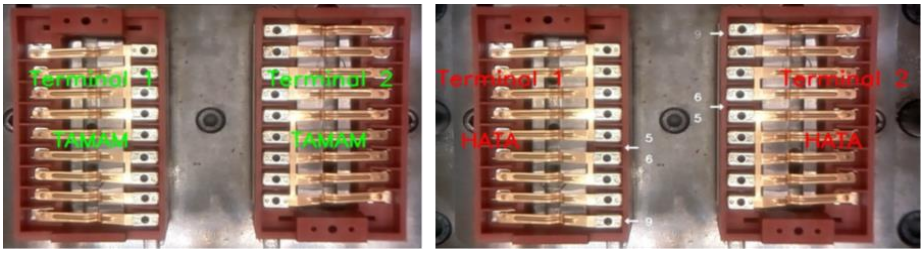

Figure 9. Pass Warning (on the left) and Defective Warning (on the right) by System

4. RESULTS AND DISCUSSION

5.000 rotary switches have been allocated for training, validation, and test of the classification algorithm. Rotary switches were processed by both human operators and the proposed system. To enhance the accuracy of the process, two operators have been visually checking for defects before the installation of the system. Hence, the accuracy of the operators shows the result of classification by two consecutive control of two operators. The main classification error of operators is the false identification of defective switches. More clearly, the operators usually could not detect defects on rotary switches. Since the switch is safety-critical, any "defective" identification by any of the operators results to classify the switch as "defective". We have checked the reliability of the decisions of operators with Kappa Statistics [33]. Table 5 includes the classifications by both operators concerning the condition of 5.000 rotary switches.

Table 5. Classification Matrix of Human Operators

		Operator 2	
		Accept	**Defect**
Operator 1	**Accept**	4244	193
	Defect	199	364

Considering the rates in Table 5, Kappa Statistics has been calculated according to the formula in Equation 2,

$$\kappa = \frac{p_o - p_e}{1 - p_e} \qquad (2)$$

where κ is the Kappa statistics, p_o is the observed agreement between operators, p_e is the hypothetical probability of chance agreement. The scale for Kappa Statistics [34] in Table 6 suggests the current classification performance of operators results in substantial agreement with a Kappa value of 61 %.

Table 6. Agreement Scale for Kappa Statistics

Kappa	**Agreement**
< 0	Less than chance agreement
0.01–0.20	Slight agreement
0.21–0.40	Fair agreement
0.41–0.60	Moderate agreement
0.61–0.80	Substantial agreement
0.81–1.00	Almost perfect agreement

The results in Table 7 prove that the proposed methodology and system improve the process by nearly 1 percent compared to the cumulative classification performance of both operators which cannot be ignored where defects are evaluated with dppm rates. Support Vector Machine (SVM) classification method has been also applied for benchmarking the proposed Decision Tree Algorithm. The results show that the proposed algorithm performs better both in the means of accuracy and runtime. For image processing, Canny Edge detection on the binarized image has been tried to be classified to compare our proposed methodology. The matching accuracy on a single image did not pass the level of 91 percent. Therefore, five images per classification have been tried to increase accuracy. The accuracy could only catch an average of 95 percent and the average runtime increased to 4.5 seconds. Besides, the match difference between

defective and acceptable rotary switches had a very low resolution with an average of 1 percent. The method was ignored for further evaluation.

Table 7. Results of The Classification Process

Type of Data	# of Items	Accuracy of Operators	Accuracy of Decision Tree	Average Runtime of Decision Tree	Accuracy of SVM	Average Runtime of SVM
Training	3500	98,80 %	99,98 %	140 ms	97,08	1,316sec
Validation	750	98,53 %	99,46 %	135 ms	95,88	1,418 sec
Test	750	98,40 %	99,60 %	135 ms	96,14	1,395 sec

Apart from featuring aspects like cost, integrability, simplicity, accessibility, etc, the proposed system should be also compared to similar systems for its performance concerning accuracy and runtime. Several similar studies have been also compared to the proposed methodology. The proposed classification algorithms by Chauhan and Surgenor [35] uses motions instead of images on a high-speed O-ring assembly line. Although having the processing power of a PLC behind, the fastest algorithm requires 5.88 seconds to process a 10-seconds video which exceeds the limit for the cycle of operation in rotary switch production line. The system should receive a defective or acceptable signal before fixing the moving terminals. Hence, it can be assessed that motion analysis for defect detection would have a risk to create a bottleneck on the production line. In another study by Kunakornvong and Sooraksa [36], the assembly of the Air Bearing Surface (ABS) is controlled via a Machine Vision System on a Hard Disk Drive (HDD). With the help of an industrial camera and industrial PC with Intel Core i7 CPU, they process the surface image of a DD by detecting defects with Fuzzy Dynamic Histogram Equalization. The average runtime for the proposed system is 2 seconds on the industrial PC. Shen et al. [37] developed a machine vision system to check defects of bearings. Their Support Vector Machine (SVM) based methodology provides also nearly 99 percent accuracy without including the runtime information. The image processing algorithm checks the smoothness and text on the body of the bearing. Edinbarough et al [38] suggested an inspection system that controls IC of PCB with a Neural Network-based algorithm. Without providing exact runtime, they provide training time as 8 – 20 minutes and 99 percent accuracy for classification.

It can be deducted from the survey that many studies focus on providing detailed information on algorithms avoiding to include runtime or accuracy statistics. As another aspect, the performance may drastically change depending on the aim of the application, required results, software and hardware environment, the number of features, type of classification, and image processing algorithms. Hence, it is assessed that the best way for developing an effective is trying to achieve the required accuracy with the simplest possible algorithm.

After integrating the visual system into the manufacturing system, the production process has been observed for one month to have more concrete results. RPN values for the risks have been updated as shown in Table 8 after attaining a stable process. Severity value could not be updated since the design of the product has not been changed. Better probability and detectability scores provided from the proposed system helped to improve overall RPN scores of the corresponding risks.

Table 8. Updated FMEA Items

P/D	Process Step/Related Part	Failure Mode	Failure Effect	Sev.	Prob.	Det.	RPN
P	Assembly of Moving Terminals by Press	Wrong Sequence	Wrong electrical functionality, should be scrapped	9	3	2	**54**

P	Assembly of Moving Terminals by Press	Wrong types of moving terminal	Wrong electrical functionality, should be scrapped	9	2	2	**36**
D	Moving Terminal	Deformed moving terminal	Avoiding functionality, should be scrapped	8	2	2	**32**

The presentation of the P/D column in the FMEA table is another contribution of this study, where P stands for Process and D stands for Design. Hence, both Design and Process items can be displayed in the same table without any confusion. Although not changing the severity, a new Poka-Yoke Device helped to improve Probability and Detection values.

5. CONCLUSION

With technological improvements, the number of cost-effective systems in the industry has been drastically increased to provide benefits on quality costs. In this study, a Raspberry Pi-based low-cost Machine Vision System that is integrated into a rotary switch manufacturing system has been presented. The system was installed to detect the type, sequence, and form defects of moving terminals before pressing on the rotary switch body. Hence, the scrap of the rotary switch was avoided by detecting the failure before pressing which is an irreversible process.

Results show that the vector inquired by thresholding and binarization operations on the image of the rotary switch was sufficient to compare default values and detect defects. Raspberry Pi-operated OpenCV software can provide the vector accurately under appropriate lighting. Classification algorithm coded on Python improves the quality control process early 1 percent compared to human operators with regards to training, validating, and testing results. 1 percent improvement on the quality control process cannot be ignored where the defect of the product is calculated with dppm level. Additionally, the same process can be completed with one operator instead of two.

The distinguishing part of the study is a combination of PFMEA and DFMEA analysis. To the best of the authors' knowledge, this is the first study that applies both PFMEA and DFMEA to determine the improvements in the quality of a manufacturing system. Another originality is the new "P/D" column for FMEA analysis which distinguishes the FMEA items as "Process" or "Design". In this way, both Process and Design items may be displayed in the same FMEA table without any confusion. During FMEA analysis, failure modes scored according to Severity, Probability, and Detectability dimensions. For future study, a new dimension as "Scope" is suggested to be added to FMEA studies for a more robust decision process. This dimension may determine the degree of relevance of failure mode to the application area.

6. ACKNOWLEDGEMENTS

The study is conducted in and supported by AN-EL Anahtar ve Elektrikli Ev Aletleri Sanayi A.S.. We thank the Top Management and R&D Center Team Members for their contributions.

7. REFERENCES

1. Hernández, B., Jiménez, J., & Martín, M. J. (2010). Customer behavior in electronic commerce: The moderating effect of e-purchasing experience. Journal of business research, 63(9-10), 964-971.

2. Gunasekaran, A. (1999). Agile manufacturing: a framework for research and development. International journal of production economics, 62(1-2), 87-105.

3. Louw, L., & Droomer, M. (2019). Development of a low cost machine vision based quality control system for a learning factory. Procedia Manufacturing, 31, 264-269.

4. Würschinger, H., Mühlbauer, M., Winter, M., Engelbrecht, M., & Hanenkamp, N. (2020). Implementation and potentials of a machine vision system in a series production using deep learning and low-cost hardware. Procedia CIRP, 90, 611-616.

5. Ardhy, F., & Hariadi, F. I. (2016, November). Development of SBC based machine-vision system for PCB board assembly automatic optical inspection. In 2016 International Symposium on Electronics and Smart Devices (ISESD) (pp. 386-393). IEEE.

6. Gong, Y., Lin, Z., Wang, J., & Gong, N. (2018). Bringing machine intelligence to welding visual inspection: development of low-cost portable embedded device for welding quality control. Electronic Imaging, 2018(9), 279-1.

7. Korodi, A., Anitei, D., Boitor, A., & Silea, I. (2020). Image-processing-based low-cost fault detection solution for end-of-line ECUs in automotive manufacturing. Sensors, 20(12), 3520.

8. Adamo, F., Attivissimo, F., Di Nisio, A., & Savino, M. (2009). A low-cost inspection system for online defects assessment in satin glass. Measurement, 42(9), 1304-1311.

9. Frustaci, F., Perri, S., Cocorullo, G., & Corsonello, P. (2020). An embedded machine vision system for an in-line quality check of assembly processes. Procedia Manufacturing, 42, 211-218.

10. Parakontan, T., & Sawangsri, W. (2019, June). Development of the Machine Vision System for Automated Inspection of Printed Circuit Board Assembl. In 2019 3rd International Conference on Robotics and Automation Sciences (ICRAS) (pp. 244-248). IEEE.

11. Di Leo, G., Liguori, C., Pietrosanto, A., & Sommella, P. (2017). A vision system for the online quality monitoring of industrial manufacturing. Optics and Lasers in Engineering, 89, 162-168.

12. Moru, D. K., & Borro, D. (2020). A machine vision algorithm for quality control inspection of gears. The International Journal of Advanced Manufacturing Technology, 106(1), 105-123.

13. Safavian, S. R., & Landgrebe, D. (1991). A survey of decision tree classifier methodology. IEEE transactions on systems, man, and cybernetics, 21(3), 660-674.

14. Song, Y. Y., & Ying, L. U. (2015). Decision tree methods: applications for classification and prediction. Shanghai archives of psychiatry, 27(2), 130.

15. Wang, C. H., Guo, R. S., Chiang, M. H., & Wong, J. Y. (2008). Decision tree based control chart pattern recognition. International Journal of Production Research, 46(17), 4889-4901.

16. Matsko, I. I., Logunova, O. S., Pavlov, V. V., & Matsko, O. S. (2012). Adaptive fuzzy decision tree with dynamic structure for automatic process control system o of continuous-cast billet production. IOSR Journal of Engineering, 2(8), 53-55.

17. Putri, N. K. S., Puika, K. S., Ibrahim, S., & Darmawan, L. (2018, September). Defect Classification Using Decision Tree. In 2018 International Conference on Information Management and Technology (ICIMTech) (pp. 281-285). IEEE.

18. Chen, J., Lian, Y., & Li, Y. (2020). Real-time grain impurity sensing for rice combine harvesters using image processing and decision-tree algorithm. Computers and Electronics in Agriculture, 175, 105591.

19. Zhou, Q., Chen, R., Huang, B., Liu, C., Yu, J., & Yu, X. (2019). An automatic surface defect inspection system for automobiles using machine vision methods. Sensors, 19(3), 644.

20. Lin, Y., Xiang, Y., Lin, Y., & Yu, J. (2019, September). Defect detection system for optical

element surface based on machine vision. In 2019 2nd International Conference on Information Systems and Computer Aided Education (ICISCAE) (pp. 415-418). IEEE.

21. Breiman, L., Friedman, J., Stone, C. J., & Olshen, R. A. (1984). Classification and regression trees. CRC press.

22. Stamatis, D. H. (2003). Failure mode and effect analysis: FMEA from theory to execution. Quality Press.

23. Agarwala, A. S. (1990, January). Shortcomings in mil-std-1629A guidelines for criticality analysis. In Annual Proceedings on Reliability and Maintainability Symposium (pp. 494-496). IEEE.

24. Office of manned space flight, Apollo program, Apollo Reliability and Quality Assurance Office. (1966). Procedure for Failure Mode, Effects and Criticality Analysis (FMECA).

25. Maddalena, S., Darmon, A., & Diels, R. (2005). Automotive CMOS image sensors. In Advanced Microsystems for Automotive Applications 2005 (pp. 401-412). Springer, Berlin, Heidelberg.

26. Klochkov, Y., Its, A., & Vasilieva, I. (2016). Development of FMEA method with the purpose of quality assessment of can stock production. In Key Engineering Materials (Vol. 684, pp. 473-476). Trans Tech Publications Ltd.

27. Sharma, K. D., & Srivastava, S. (2018). Failure mode and effect analysis (FMEA) implementation: a literature review. J. Adv. Res. Aeronaut. Space Sci, 5, 1-17.

28. Spreafico, C., Russo, D., & Rizzi, C. (2017). A state-of-the-art review of FMEA/FMECA including patents. Computer Science Review, 25, 19-28.

29. Huang, J., You, J. X., Liu, H. C., & Song, M. S. (2020). Failure mode and effect analysis improvement: A systematic literature review and future research agenda. Reliability Engineering & System Safety, 106885.

30. Ng, W. C., Teh, S. Y., Low, H. C., & Teoh, P. C. (2017, September). The integration of FMEA with other problem solving tools: A review of enhancement opportunities. In J Phys Conf Ser (Vol. 890, p. 012139).

31. AIAG-VDA FMEA Handbook 4. Edition (2019)

32. Puvanasvaran, A. P., Jamibollah, N., Norazlin, N., & Adibah, R. (2014). Poka-Yoke Integration into process FMEA. Australian Journal of Basic and Applied Sciences, 8(7), 66-73.

33. Cohen, J. (1960). A coefficient of agreement for nominal scales. Educational and psychological measurement, 20(1), 37-46.

34. Viera, A. J., & Garrett, J. M. (2005). Understanding interobserver agreement: the kappa statistic. Fam med, 37(5), 360-363.

35. Chauhan, V., & Surgenor, B. (2015). A comparative study of machine vision based methods for fault detection in an automated assembly machine. Procedia Manufacturing, 1, 416-428.

36. Kunakornvong, P., & Sooraksa, P. (2016). Machine vision for defect detection on the air bearing surface. In 2016 International Symposium on Computer, Consumer and Control (IS3C) (pp. 37-40). IEEE.

37. Shen, H., Li, S., Gu, D., & Chang, H. (2012). Bearing defect inspection based on machine vision. Measurement, 45(4), 719-733.

38. Edinbarough, I., Balderas, R., & Bose, S. (2005). A vision and robot based on-line inspection monitoring system for electronic manufacturing. Computers in Industry, 56(8-9), 986-996.

DOI: 10.38061/idunas.932338

IDUNAS	NATURAL & APPLIED SCIENCES JOURNAL	2021 Vol. 4 No. 2 (16-31)

Infinite Perimeter Selective Segmentation Model

Research Article

Lavdie Rada[1*]

[1]Biomedical Engineering Department, Bahcesehir University, Istanbul, Turkey.

Author E-mails
lavdie.rada@eng.bau.edu.tr

*Correspondance to: Lavdie Rada, Biomedical Engineering Department, Bahcesehir University, Istanbul, Turkey.
DOI: 10.38061/idunas.932338

Received:, 03.06.2021; Accepted: 05.11.2021

Abstract

Accurate boundary determination and segmentation of an object of interest in an image is a difficult image segmentation task. In this paper, we propose a new variational model composed of two penalizations and two fitting terms improving the old selective segmentation models. To better deal with oscillatory boundaries, a $\mathcal{H}^1$ weighted length term and $\mathcal{L}^2$ Lebesgue measure have been employed as penalization terms, whereas the fitting terms consist of a region-based and area fitting term. The model has the same speed as the previous one-level set interactive segmentation models and is much faster compared to previously dual-level set models by having the same segmentation accuracy and reliability. On the other hand, the model shows a good performance while dealing with irregular and oscillatory object boundaries. The comparison with segmentation algorithms of the same nature shows that the proposed model shows the same or improved performance for object segmentation with transparent boundaries or inhomogeneous intensity of the aimed object. Moreover, we show that the proposed model finds the aimed object boundaries successfully for smooth or challenging oscillatory topological structures.
Keywords: Total variation, Edge detection, $\mathcal{L}^2$-Lebesgue measure, Interactive segmentation.

1. INTRODUCTION

Despite developments and improvements in photography and imaging, image post-processing techniques are commonly required. Image segmentation is one such task that separates the object/ objects from their surroundings by extracting aimed boundaries in a meaningful manner. Many applications of image segmentation are observed in a wide range of fields, such as medical imaging, object detection and recognition, traffic control systems, etc.

Segmentation techniques divide into two classes: global and selective/interactive segmentation. The first class aims at the boundary of all objects into a given image scene, whereas the second class aims at the boundary of a specific object. Global segmentation consists of objects' boundaries extraction (foreground) from their surrounding (background). In the last decades, different global segmentation techniques, such as

region-based segmentation, edge-based segmentation, clustering, Mask R-CNN, etc., have been introduced. Variational segmentation models, based on an early idea of representing the image as a piece-wise continuous function [19], easily implemented by Chan-Vese (CV) [7] through the level set function [22], was further used by many segmentation techniques. CV model and further followed improved models prove to be very efficient compared with statistical methods [10, 9, 30], image thresholding [16, 26], wavelet techniques [17, 14,27], etc. Most variational based segmentation approaches in the last decades base their models on edge information to guide the contours towards aimed edges [1, 6, 11, 13] or statistical information for the homogeneous area in the object's region, similar to the CV model [7].

On the other hand, in some particular applications, one single object is required to be segmented. Such examples can be found in medical imaging where a particular organ is required to automatically be segmented or Closed Circuit TV (CCTV) surveillance system where activities monitoring is aimed. The main issue in an interactive/ selective image segmentation problem is how to distinguish one object of interest from similar (nearby) other objects. Recently, variational based models were proposed [3, 13, 18, 25, 24]. Those models combine edge detection function with distance metrics to form some geometric priors information (markers). Such work was introduced by Rada et al. [25] where a dual-level set is used for boundaries detection (a local level set evolves over a global level set to detect the boundaries on the aimed target object). The model show improvement compared to other models of the same type by being more reliable for cases where the intensity difference between objects is small. Although this model [25] is reliable, the model does not perform well for oscillatory boundaries. To improve the model for such boundaries a new dual-level set model was introduced by the same authors [24]. The new model [24] improves the old model by using the $\mathcal{L}^2$ Lebesgue measure of the γ-neighborhood of the contour [4] replacing the $\mathcal{H}^1$ Hausdorff measure [25] as penalization term. Both these models are slow because of the complexity of the incorporation of the two level set functions. To improve the dual-level set work [25], Rada et al. [24] introduced a new variational area fitting based model. This model is fast and reliable but has slight difficulties with specific cases where the aimed objects have oscillatory boundaries. The purpose of the following presented work consist of the design of a new single level-set model which yet ensuring the same or better performance for oscillatory boundaries compared to Rada et al. [24] model.

Furthermore, we should emphasize that for image data where prior information is provided different machine learning and pattern recognition algorithms can be employed [5, 2, 8]. However, their large training sets and parameters optimization through the architecture layers makes them limited for previously unseen object classes. In this paper, we consider the cases where prior data is not available and the method can be easily adapted for general cases.

The following sections are organized in the following way. Section 2 contains a review of some selective segmentation models. In Section 3, we present the proposed $\mathcal{L}^2$ Lebesgue measure based model. Then, in Section 4, the discretization of the derived partial differential question through an additive operator splitting (AOS) algorithm is described, ist efficiency and speed. In Section 5, we provide experimental results and comparisons to some existing methods for different images. We conclude our work in Section 6.

2. A SHORT REVIEW ON SOME INTERACTIVE/SELECTIVE SEGMENTATION MODELS

The introduction of a level set idea by Chan-Vese (CV) [7] led to a simple and easy numerical representation of the Mumford-Shah [20] variational image segmentation model. Using Chan-Vese (CV) [7] idea many segmentation models were introduced in the last decades. Given an image $u_0(\boldsymbol{x})$, $x \in \Omega$ defined on a rectangular domain Ω, the CV model restricts the image into a piecewise function to be

represented with a two-phase level set function. The piecewise function consists of two values c_1 and c_2 that represent the mean intensity value of the foreground and the background, respectively. The CV model is not based on the gradient of the image for the stopping process so that it can detect contours both with and without gradients. The energy minimization functional in terms of level set is given as follows:

$$\min_{c_1,c_2,\Gamma} F(\Gamma, c_1, c_2) = \min_{c_1,c_2,\Gamma} \{\mu_{cv}\text{length}(\Gamma) + \lambda_{1cv} \int_{\text{inside }(\Gamma)} |u_0(\mathbf{x}) - c_1|^2 d\mathbf{x}$$

$$+ \lambda_{2cv} \int_{\text{outside }(\Gamma)} |u_0(\mathbf{x}) - c_2|^2 d\mathbf{x}\} \quad (1)$$

where c_1 and c_2 are the average values of $u_0(\boldsymbol{x})$ inside and outside of the variable contour Γ, also μ, λ_1 and λ_2 are non-negative fixed parameters. Writing the level set function $\phi: \Omega \to \mathbb{R}$

$$\begin{cases} \Gamma = \partial\Omega_1 = \{(\boldsymbol{x}) \in \Omega |\ \phi(\boldsymbol{x}) = 0\}, \\ \text{inside}(\Gamma) = \Omega_1 = \{\boldsymbol{x} \in \Omega |\ \phi(\boldsymbol{x}) > 0\}, \\ \text{outside}(\Gamma) = \Omega_2 = \{\boldsymbol{x} \in \Omega |\ \phi(\boldsymbol{x}) < 0\}, \end{cases}$$

the energy function (1) is written in the form:

$$F(\phi, c_1, c_2) = \mu_{cv} \int_\Omega |\nabla H(\phi)| d\boldsymbol{x} + \lambda_{1cv} \int_\Omega |u_0(\boldsymbol{x}) - c_1|^2 H\big(\phi(\boldsymbol{x})\big) d\boldsymbol{x}$$
$$+\lambda_{2cv} \int_\Omega |u_0(\boldsymbol{x}) - c_2|^2 (1 - H(\phi(\boldsymbol{x}))) d\boldsymbol{x}, \quad (2)$$

where H defines the Heaviside function

$$H(x) = \begin{cases} 1 & \text{if } x \geq 0 \\ 0 & \text{if } x < 0. \end{cases}$$

In the following we review selective segmentation models related to the new proposed work.

Dual Level Set Selective Segmentation Model for Oscillatory Boundaries With Infinite Perimeter Norm

As an attempt to improve the dual level set model [25] for segmentation of objects with irregular boundaries, the work of Rada et al. [24] replaces the $\mathcal{H}^1$ length term in the old Rada et al. work [25] with the γ-neighborhood area of the contour Γ (following the Barchiesi et al. [4] approach for global segmentation). The γ-neighborhood area of the contour of the edge set Γ is given as follows [4]

$$\gamma - \Gamma := \cup_{x \in \Gamma} B_\gamma(x). \quad (3)$$

This $\mathcal{L}^2$ measure plays an important role in capturing inperfect oscillating boundaries boundaries of the foregrownd objects in the given image $u_0(x)$ while achieving the denoising effect [4]. Considering $f_0 := \chi_{0,1]}$, and a smooth version of it f, such as $f(t) = e^{-t^k}$ or $f(t) = \frac{1}{1+t^k}$ for $k \geq 1$, the $\mathcal{L}^2(\gamma - \Gamma)$ term can be rewritten as:

$$\mathcal{L}^2(\gamma - \Gamma) := \int_\Omega f_0\left(\frac{dist\,(x,\Gamma)}{\gamma}\right) dx \approx \int_\Omega f\left(\frac{dist\,(x,\Gamma)}{\gamma}\right) dx. \quad (4)$$

In the presented work of Rada et al. [24], the $\mathcal{L}^2(\gamma - \Gamma)$ is approximated as

$$\mathcal{L}^2(\gamma - \Gamma) \approx \int_\Omega e^{-\frac{\phi(h)^k}{\gamma^k}},$$

for large value of the parameter k. Following similar problem to the level set selective segmentation models [3, 11, 13, 25], a set of geometrical points $\mathcal{A} = \{w_i^* = (x_i^*, y_i^*) \in \Omega, 1 \leq i \leq n_1\} \subset \Omega$, consisting of n_1 distinct points near the object, has been defined. Using the Lipschitz level set function the energy function of this model is given as following:

$$\min_{\phi_L(\mathbf{x}),\phi_G(\mathbf{x}),c_1,c_2} F_{IDLSS}(\phi_L,\phi_G,c_1,c_2) =$$
$$\mu_1 \int_\Omega D(\mathbf{x})g(\nabla u_0)e^{-(\frac{\phi_L}{\gamma})^k} H(\phi_G) + \frac{\mu_L}{2}\int_\Omega (|\nabla\phi_L| - 1)^2 d\mathbf{x} \; +$$
$$\mu_2 \int_\Omega g(\nabla u_0)e^{-(\frac{\phi_G}{\gamma})^k} + \frac{\mu_G}{2}\int_\Omega (|\nabla\phi_G(\mathbf{x})| - 1)^2 d\mathbf{x} \; + \qquad (5)$$
$$\lambda_{1G}\int_\Omega |u_0(\mathbf{x}) - c_1|^2 H(\phi_G(\mathbf{x})d\mathbf{x} \; + \lambda_{2G}\int_\Omega |u_0(\mathbf{x}) - c_2|^2(1 - H(\phi_G(\mathbf{x}))d\mathbf{x} \; +$$
$$\lambda_1 \int_\Omega |u_0(\mathbf{x}) - c_1|^2 H(\phi_L(\mathbf{x})d\mathbf{x} \; + \lambda_2 \int_\Omega |u_0(\mathbf{x}) - c_1|^2(1 - H)(\phi_L(\mathbf{x}))H(\phi_G(\mathbf{x})d\mathbf{x} \; +$$
$$\lambda_3 \int_\Omega |u_0(\mathbf{x}) - c_2|^2(1 - H)(\phi_L(\mathbf{x}))(1 - H(\phi_G(\mathbf{x}))d\mathbf{x}.$$

where ϕ_L, ϕ_G, are the local level set and global level set, respectively, $D(\mathbf{x})$ and $g(\mathbf{x})$, are the distance and edge detection functions, respectively. Both $D(\mathbf{x})$ and $g(\mathbf{x})$ function has a property of approaching zero while aproaching near the Γ boundary and has big value when away from it. The global level set detect all the boundaries of the objects in the given image whereas the local level set evolves over the global level set in order to detect the aimed object near the given geometric set of points. The constants $\mu_1, \mu_2, \lambda_{1G}, \lambda_{2G}, \mu_L, \mu_G, \lambda_1, \lambda_2, \lambda_3$, are defined parameters related to the model. The functions $H(\phi_L)$, and $H(\phi_G)$ represent the local and global level set functions corresponding to the local and global level set.

To tackle the discontinuity issue in 0 of the Heaviside function, regularized Heaviside functions can be used such as $H_\epsilon = \frac{1}{2}(1 + \frac{2}{\pi}\arctan(\frac{z}{\epsilon}))$. In this way the above model can be written:

$$\min_{\phi_L(\mathbf{x}),\phi_G(\mathbf{x}),c_1,c_2} F_{IDLSS}(\phi_L,\phi_G,c_1,c_2) =$$
$$\mu_1 \int_\Omega D(\mathbf{x})g(\nabla u_0)e^{-(\frac{\phi_L}{\gamma})^k} H_\epsilon(\phi_G) + \frac{\mu_L}{2}\int_\Omega (|\nabla\phi_L| - 1)^2 d\mathbf{x} \; +$$
$$\mu_2 \int_\Omega g(\nabla u_0)e^{-(\frac{\phi_G}{\gamma})^k} + \frac{\mu_G}{2}\int_\Omega (|\nabla\phi_G(\mathbf{x})| - 1)^2 d\mathbf{x} \; + \qquad (6)$$
$$\lambda_{1G}\int_\Omega |u_0(\mathbf{x}) - c_1|^2 H_\epsilon(\phi_G(\mathbf{x})d\mathbf{x} \; + \lambda_{2G}\int_\Omega |u_0(\mathbf{x}) - c_2|^2(1 - H_\epsilon(\phi_G(\mathbf{x}))d\mathbf{x} \; +$$
$$\lambda_1 \int_\Omega |u_0(\mathbf{x}) - c_1|^2 H_\epsilon(\phi_L(\mathbf{x})d\mathbf{x} \; + \lambda_2 \int_\Omega |u_0(\mathbf{x}) - c_1|^2(1 - H_\epsilon(\phi_L(\mathbf{x}))H(\phi_G(\mathbf{x})d\mathbf{x} \; +$$
$$\lambda_3 \int_\Omega |u_0(\mathbf{x}) - c_2|^2(1 - H_\epsilon(\phi_L(\mathbf{x}))(1 - H_\epsilon(\phi_G(\mathbf{x}))d\mathbf{x}.$$

By keeping ϕ_L and ϕ_G fixed and deriving with respect to c_1 and c_2, one get equations for computing c_1 and c_2:

$$c_1 = \frac{\lambda_{1G}\int_\Omega u_0 H_\epsilon(\phi_G)d\mathbf{x} + \lambda_1\int_\Omega u_0 H_\epsilon(\phi_L)d\mathbf{x} + \lambda_2\int_\Omega u_0(1 - H_\epsilon(\phi_L))H_\epsilon(\phi_G)d\mathbf{x}}{\lambda_{1G}\int_\Omega H_\epsilon(\phi_G)d\mathbf{x} + \lambda_1\int_\Omega H_\epsilon(\phi_L)d\mathbf{x} + \lambda_2\int_\Omega (1 - H_\epsilon(\phi_L))H_\epsilon(\phi_G)d\mathbf{x}}, \qquad (7)$$

$$c_2 = \frac{\lambda_{2G}\int_\Omega u_0(1 - H_\epsilon(\phi_G))d\mathbf{x} + \lambda_3\int_\Omega u_0(1 - H_\epsilon(\phi_L))(1 - H_\epsilon(\phi_G))d\mathbf{x}}{\lambda_{2G}\int_\Omega (1 - H_\epsilon(\phi_G))d\mathbf{x} + \lambda_3\int_\Omega (1 - H_\epsilon(\phi_L))(1 - H_\epsilon(\phi_G))d\mathbf{x}}, \qquad (8)$$

and by keeping c_1 and c_2 fixed we get the equations for ϕ_G and ϕ_L

$$\begin{cases} \mu_2 g(\nabla u_0)\frac{k}{\gamma^k}\phi_G^{k-1}e^{-(\frac{\phi_G}{\gamma})^k} + \mu_G\nabla\cdot((1-\frac{1}{|\nabla\phi_G|})\nabla\phi_G) + \\ \delta_\epsilon(\phi_G)(-\mu_1 d(\mathbf{x})g(\nabla u_0)e^{-(\frac{\phi_L}{\gamma})^k} - \lambda_{1G}(u_0(\mathbf{x})-c_1)^2 + \lambda_{2G}(u_0(\mathbf{x})-c_2)^2 - \\ \lambda_2(u_0(\mathbf{x})-c_1)^2(1-H(\phi_L)) + \lambda_3(u_0(\mathbf{x})-c_2)^2(1-H(\phi_L))) \;+\; \alpha g(\mathbf{x})|\nabla\phi_G| = 0, \text{in } \Omega \\ \frac{\partial\phi_G}{\partial\vec{n}} = 0 \text{ on } \partial\Omega. \end{cases} \tag{9}$$

and

$$\begin{cases} \mu_1 D(\mathbf{x})g(\nabla u_0)\frac{k}{\gamma^k}\phi_L^{k-1}e^{-(\frac{\phi_L}{\gamma})^k}H_\epsilon(\phi_G) + \mu_L\nabla\cdot((1-\frac{1}{|\nabla\phi_L|})\nabla\phi_L) + \\ \delta_\epsilon(\phi_L)(-\lambda_1(u_0(\mathbf{x})-c_1)^2 + \lambda_2(u_0(\mathbf{x})-c_1)^2 H_\epsilon(\phi_G) + \\ \lambda_3\left(u_0(\mathbf{x})-c_2)^2(1-H_\epsilon(\phi_G)\right)\right) \;+\; \alpha d(\mathbf{x})g(\nabla u_0)|\nabla\phi_L| = 0, \text{in}\Omega \\ \frac{\partial\phi_L}{\partial\vec{n}} = 0 \text{ on } \partial\Omega, \end{cases} \tag{10}$$

The terms $\alpha g(x,y)|\nabla\phi_G|$ and $\alpha d(x,y)g(\nabla u_0)|\nabla\phi_L|$ are the balloon term force.

Area Based Selective Segmentation Model

Rada et al. [23] introduced a simple and fast variational model for the interactive/ selective segmentation task. This model improved the old dual-level set model [25]. This method is based on a Euclidean distance from the manually given points combined with an area-based fitting term and an adaptive parameter edge detection function, which tends to 0 as soon as the contour reaches the boundaries. Given an image $u_0(x)$, defined on the domain Ω, the detection of an aimed feature/object nearby some given points $\mathcal{A} = \{w_i^* = (x_i^*, y_i^*) \in \Omega, 1 \le i \le n_1\} \subset \Omega$, is given in the following form:

$$\begin{aligned} \min_{\Gamma,c_2} F(\Gamma, c_2) \;&= \min_{\Gamma,c_2}\{\mu\int_\Gamma W(|\nabla u_0(\mathbf{x})|)d\mathbf{x} \;+ \\ &\lambda_1\int_{inside\,(\Gamma)}|u_0(\mathbf{x})-c_1|^2 d\mathbf{x} \;+\lambda_2\int_{outsite\,(\Gamma)}|u_0(\mathbf{x})-c_2|^2 d\mathbf{x} \;+ \\ &\nu\{(\int_{inside\,(\Gamma)} d\mathbf{x} - A_1)^2 + (\int_{outsite\,(\Gamma)} d\mathbf{x} - A_2)^2\}, \end{aligned} \tag{11}$$

where $\lambda_1, \lambda_2, \mu$ and ν are empirical weights, $W = D \cdot g$ is the edge detector distance function, c_1 is the mean intensity of constructed polygon with the given points, c_2 is a region term representing the mean intensity outside the target object. The area fitting term, represented in the last row of the last equation, tend to minimize the difference between the area obtained by the evolving level set of the aimed object and the approximated area obtained by the polygon of the given geometric markers. This term serves as a ration constraint between the aimed object and the rest of the image rather than precise area-preserving. The function g is an edge detection function given by:

$$g(|\nabla u_0(\mathbf{x})|) = \frac{1}{1+k|\nabla u_0(\mathbf{x})|^2}, \tag{12}$$

with k a positive constant which can be manualy adapted. Replacing the Heaviside function H with a continuous regularized function H_ϵ, similar to [1, 7] one get:

$$\min_{\phi(x),c_2} F_\epsilon(\phi(\boldsymbol{x}),c_2) = \mu\int_\Omega W(|\nabla u_0(\boldsymbol{x})|)\delta_\epsilon(\phi(\boldsymbol{x}))|\nabla(\phi(\boldsymbol{x}))|d\boldsymbol{x} + \lambda_1\int_\Omega |u_0(\boldsymbol{x})-c_1|^2 H_\epsilon(\phi(\boldsymbol{x}))d\boldsymbol{x} + \lambda_2\int_\Omega |u_0(\boldsymbol{x})-c_2|^2(1-H_\epsilon(\phi(\boldsymbol{x})))d\boldsymbol{x} + \nu\{(\int_\Omega H_\epsilon(\phi(\boldsymbol{x}))d\boldsymbol{x}-A_1)^2 + (\int_\Omega (1-H_\epsilon(\phi(\boldsymbol{x}))d\boldsymbol{x})-A_2)^2\}d\boldsymbol{x}, \quad (13)$$

where $\delta_\epsilon(\phi(\boldsymbol{x}))$ is a Delta function corresponding to the Heaviside function introduced above. Considering that the geometrical points are given inside the aimed object c_1 is computed as the mean intensity of the constructed polygon with those points. Keeping $\phi(x)$ fixed and minimizing with respect to the unknown intensity outside the object, one gets the following equations for computing c_2:

$$c_2(\phi(\boldsymbol{x})) = \frac{\int_\Omega u_0(\boldsymbol{x})(1-H_\epsilon(\phi(\boldsymbol{x})))d\boldsymbol{x}}{\int_\Omega (1-H_\epsilon(\phi(\boldsymbol{x})))d\boldsymbol{x}} \quad (14)$$

if $\int_\Omega (1-H_\epsilon(\phi(\boldsymbol{x})))d\boldsymbol{x} > 0$ (i.e if the curve is nonempty in Ω).

Considering c_1 and c_2 fixed and minimizing (18) with respect to $\phi(\boldsymbol{x})$ and get the following Euler-Lagrange equation:

$$\delta_\epsilon(\phi)\{\mu\nabla\cdot(W\frac{\nabla\phi}{|\nabla\phi|}) - [\lambda_1(u_0(\boldsymbol{x})-c_1)^2 - \lambda_2(u_0(\boldsymbol{x})-c_2)^2] - \nu[(\int_\Omega H d\mathbf{x}-A_1) - (\int_\Omega (1-H)d\mathbf{x}-A_2)]\} = 0, \text{in}\Omega \quad (15)$$
$$\text{with}\frac{\partial\phi}{\partial\vec{n}} = 0, \text{on}\partial\Omega,$$

To speed up the convergence in equation (20) a balloon term, such as $\alpha W|\nabla\phi|$, can be optionaly added. The final equations of ϕ can be written in the form:

$$\delta_\epsilon(\phi)\{\mu\nabla\cdot(W\frac{\nabla\phi}{|\nabla\phi|}) - [\lambda_1(u_0(\boldsymbol{x})-c_1)^2 - \lambda_2(u_0(\boldsymbol{x})-c_2)^2] - \nu[(\int_\Omega H d\mathbf{x}-A_1) - (\int_\Omega (1-H)d\mathbf{x}-A_2)]\} - \alpha W|\nabla\phi| = 0. \quad (16)$$

3. PROPOSED METHOD

In this section, we detail the proposed single level selective segmentation model, useful for oscillatory boundaries which has a better speed performance compared to the previously proposed dual level set model [24]. For a given image $u_0(\mathbf{x})$, defined on the domain Ω, we aim to detect a feature/object of an image nearby the geometrical marked points $\mathcal{A}$, placed nearby the aimed object boundaries. To achieve a correct detection of the aimed irregular boundary object we incorporate: i) a distance-edge detection function incorporated in the smoothing term providing a value $\simeq 0$ while approaching the aimed object; ii) an area-based fitting term providing conditioning the detected area to be is in the same range with the aimed object; iii) an $\mathcal{L}^2$-Lebesgue length term evaluating the area of the γ −neighborhood of the edge set Γ capable to deal with noise, preserve the cornering effect and keeping oscillatory boundaries; iv) $\mathcal{H}^1$ weighted length of the contour. The proposed model is given in the following form:

$$\min_{\Gamma,c_2} F(\Gamma,c_2) = \min_{\Gamma,c_2}\{\mu\int_\Gamma W(|\nabla u_0(\mathbf{x})|)d\mathbf{x} + \mu_1\int_\Omega f(\frac{dist(\mathbf{x},\Gamma)}{\gamma})d\mathbf{x} + \lambda_1\int_{inside(\Gamma)} |u_0(\mathbf{x})-c_1|^2 d\mathbf{x} + \lambda_2\int_{outsite(\Gamma)} |u_0(\mathbf{x})-c_2|^2 d\mathbf{x} + \quad (17)$$

$$\nu\{(\int_{inside\ (\Gamma)} d\mathbf{x} - A_1)^2 + (\int_{outsite\ (\Gamma)} d\mathbf{x} - A_2)^2\},$$

where $\mu, \mu_1, \lambda_1, \lambda_2$ and ν are empirical weights, $W = D \cdot g$ is the edge detector distance function, c_1 is the mean intensity of the constructed polygon with the given markers, c_2 is a region term defined in equation (14) representing the mean intensity outside the target object. As the level set function becomes irregular during computation, optionaly, one can add a fitting terms in order to avoid reinitialization of the level set function $\phi(\mathbf{x})$, e.g. the term $\int_\Omega (|\nabla\phi(\boldsymbol{x})| - 1)^2$ provides the authomatic scale of the level set.

Compering to [23] model one can notice the that the above energy improves [23] model by adding a term similar to the work of [4], capable to deal with oscillatory boundaries. Rewriting the above equation in terms of the level-set, replacing the Heaviside function with the regularized Heaviside function H_ϵ similar to [1, 7], and adding the reinatioalization term for the ϕ level set one get:

$$\begin{aligned}\min_{\phi(x),c_2} F(\phi(\boldsymbol{x}), c_2) \quad &= \mu \int_\Omega g(|\nabla u_0(\boldsymbol{x})|)|\nabla H_\epsilon(\phi(\boldsymbol{x}))|d\boldsymbol{x} + \\ &\mu_1 \int_\Omega G(|\nabla u_0(\mathbf{x})|)g(\nabla u_0)e^{-\frac{\phi^k}{\gamma}} d\mathbf{x} + \mu_2 \int_\Omega (|\nabla\phi(\boldsymbol{x})| - 1)^2 + \\ &\lambda_1 \int_\Omega |u_0(\boldsymbol{x}) - c_1|^2 H_\epsilon(\phi(\boldsymbol{x}))d\boldsymbol{x} \ + \lambda_2 \int_\Omega |u_0(\boldsymbol{x}) - c_2|^2(1 - H_\epsilon(\phi(\boldsymbol{x})))d\boldsymbol{x} + \\ &\nu\{(\int_\Omega H_\epsilon(\phi(\boldsymbol{x}))d\boldsymbol{x} - A_1)^2 + (\int_\Omega (1 - H_\epsilon(\phi(\boldsymbol{x}))d\boldsymbol{x}) - A_2)^2\}d\boldsymbol{x}. \end{aligned} \tag{18}$$

if $\int_\Omega (1 - H_\epsilon(\phi(x)))dx > 0$. Keeping ϕ fixed we update

$$c_2(\phi(\boldsymbol{x})) = \frac{\int_\Omega u_0(\boldsymbol{x})(1 - H_\epsilon(\phi(\boldsymbol{x})))d\boldsymbol{x}}{\int_\Omega (1 - H_\epsilon(\phi(\boldsymbol{x})))d\boldsymbol{x}}. \tag{19}$$

Keeping c_1 and c_2 fixed and minimizing (18) with respect to $\phi(\boldsymbol{x})$ one gets the following equation:

$$\begin{aligned}\delta_\epsilon(\phi)\{\mu\nabla \cdot (W\frac{\nabla\phi}{|\nabla\phi|}) + \quad &\mu_1 \frac{k}{\gamma^k}\phi^{k-1}e^{-(\frac{\phi}{\gamma})^k} H_\epsilon + \mu_2\nabla \cdot ((1 - \frac{1}{|\nabla\phi|})\nabla\phi) - \\ &[\lambda_1(u_0(\boldsymbol{x}) - c_1)^2 - \lambda_2(u_0(\boldsymbol{x}) - c_2)^2] - \\ &\nu[(\int_\Omega H d\mathbf{x} - A_1) - (\int_\Omega (1 - H)d\mathbf{x} - A_2)]\} = 0, \text{in}\Omega \\ &\text{with}\ \frac{\partial\phi}{\partial\vec{n}} = 0, \text{on}\partial\Omega,\end{aligned} \tag{20}$$

4. METHOD DISCRETIZATION AND SOLUTION THROUGH AN ADDITIVE OPERATOR

To solve equation (20), we employ an additive operator splitting (AOS) method known for its properties of fast and low computational cost. AOS splits the two-dimensional problem into the solution of sequential of two one-dimensional ones. The AOS method is proposed by Tai et al. [15] and Weickert [29] has been widely applied in similar diffusion equations, see [3, 13, 28]. In the following, we detail the implementation of the AOS algorithm for the proposed method. The first step of the AOS method is the discretization of the given minimization problem in equation (20). In our work central finite differences has been used. Then form a semi-implicit linear system which leads to an iterative approximation scheme with a tridiagonal diagonally dominant matrix. Recalling equation (20) of the proposed method one can write the gradient descent method as follows:

$$\begin{cases}\phi(\mathbf{x},0)=\phi^0(\mathbf{x})\\ \frac{\partial\phi}{\partial t}=\mu\delta_\epsilon(\phi)\nabla\cdot(W\frac{\nabla\phi}{|\nabla\phi|})+\mu_1\frac{k}{\gamma^k}\phi_G^{k-1}e^{-(\frac{\phi_G}{\gamma})^k}+\mu_2\nabla\cdot((1-\frac{1}{|\nabla\phi|})\nabla\phi)+\\ \delta_\epsilon(\phi)\{-[\lambda_1(u_0(\mathbf{x})-c_1)^2-\lambda_2(u_0(\mathbf{x})-c_2)^2]-\\ \nu[(\int_\Omega Hd\mathbf{x}-A_1)-(\int_\Omega(1-H)d\mathbf{x}-A_2)]\}=0,\end{cases} \tag{21}$$

As singularity may be shown, due to the $|\nabla\phi|$ term in the denominator, we replace the term with $|\nabla\phi|_\beta=\sqrt{\phi_x^2+\phi_y^2+\beta}$, for a small β. Denoting $E=\frac{W}{|\nabla\phi|_\beta}, F=1-\frac{1}{|\nabla\phi|}$ and

$$\begin{aligned}f=\ &\mu_1\frac{k}{\gamma^k}\phi^{k-1}e^{-(\frac{\phi}{\gamma})^k}+\delta_\epsilon(\phi)\{-[\lambda_1(u_0(\mathbf{x})-c_1)^2-\lambda_2(u_0(\mathbf{x})-c_2)^2]\ -\\ &\nu[(\int_\Omega Hd\mathbf{x}-A_1)-(\int_\Omega(1-H)d\mathbf{x}-A_2)]\}\end{aligned} \tag{22}$$

equations (21) can be written in the compact form:

$$\begin{cases}\frac{\partial\phi}{\partial t}=\mu\delta_\epsilon(\phi)\nabla\cdot(E\nabla\phi)+\mu_2\nabla\cdot(F\nabla\phi)+f=\\ \mu\delta_\epsilon(\phi)(\partial_x(E\partial_x\phi)+\partial_y(E\partial_y\phi))+\mu_2\delta_\epsilon(\phi)(\partial_x(F\partial_x\phi)+\partial_y(F\partial_y\phi))+f.\end{cases} \tag{23}$$

Discretizing respect to time the equation (23) can be rewritten in the matrix-vector form:

$$\frac{\phi^{n+1}-\phi^n}{\Delta t}=\sum_{l=1}^2 A_l(\phi^n)\phi^{n+1}+f$$

where Δt is the time step size, n denotes the n^{th} iteration and A_l is the diffusion quantity in the l direction ($l=1$ and $l=2$ respectively for x and y direction for the two dimensional case). The above equation can be written in the semi-implicit form:

$$\phi^{n+1}=(\ I-\Delta t\sum_{l=1}^m A_l(\phi^n))^{-1}\hat{\phi}^n \text{ for } l=1,2 \text{ and } \widehat{\phi}^n=\phi^n+\Delta t f.$$

Using the AOS scheme and its additively split the above equation can be written:

$$\phi^{n+1}=\frac{1}{2}\sum_{l=1}^2(\ I-2\Delta t A_l(\phi^n))^{-1}\hat{\phi}^n \tag{24}$$

Here the matrices A_l, for $l=1,2$, are obtained by using the finite differences scheme as bellow:

$$(A_1(\phi^n)\phi^{n+1})_{i,j}=\mu\delta_\epsilon(\phi^n)(\partial_x(E\partial_x\phi^{n+1})_{i,j}+\mu_2(\partial_x(F\partial_x\phi^{n+1})_{i,j}=$$

$$\mu\delta_\epsilon(\phi^n)\frac{E^n_{i+\frac{1}{2},j}(\partial_x\phi^{n+1})_{i+\frac{1}{2},j}-E^n_{i-\frac{1}{2},j}(\partial_x\phi^{n+1})_{i-\frac{1}{2},j}}{h_x}+$$

$$\mu_2\frac{F^n_{i+1/2,j}(\partial_x\phi^{n+1})_{i+1/2,j}-F^n_{i-1/2,j}(\partial_x\phi^{n+1})_{i-1/2,j}}{h_x}+$$

$$\mu\delta_\epsilon(\phi^n)\frac{\frac{E^n_{i+1,j}+E^n_{i,j}}{2}(\frac{\phi^{n+1}_{i+1,j}-\phi^{n+1}_{i,j}}{h_x})-\frac{E^n_{i,j}+E^n_{i-1,j}}{2}(\frac{\phi^{n+1}_{i,j}-\phi^{n+1}_{i-1,j}}{h_x})}{h_x}+$$

$$\mu_2 \frac{\frac{F^n_{i+1,j}+F^n_{i,j}}{2}\left(\frac{\phi^{n+1}_{i+1,j}-\phi^{n+1}_{i,j}}{h_x}\right)-\frac{F^n_{i,j}+F^n_{i-1,j}}{2}\left(\frac{\phi^{n+1}_{i,j}-\phi^{n+1}_{i-1,j}}{h_x}\right)}{h_x} =$$

$$\mu\delta_\epsilon(\phi^n)\frac{E^n_{i+1,j}+E^n_{i,j}}{2h_x^2}(\phi^{n+1}_{i+1,j}-\phi^{n+1}_{i,j})-\mu\delta_\epsilon(\phi^n)\frac{E^n_{i,j}+E^n_{i-1,j}}{2h_x^2}(\phi^{n+1}_{i,j}-\phi^{n+1}_{i-1,j})+$$

$$\mu_2\frac{F^n_{i+1,j}+F^n_{i,j}}{2h_x^2}\left(\phi^{n+1}_{i+1,j}-\phi^{n+1}_{i,j}\right)-\mu_2\frac{F^n_{i,j}+F^n_{i-1,j}}{2h_x^2}\left(\phi^{n+1}_{i,j}-\phi^{n+1}_{i-1,j}\right),$$

with A_1 is a tridiagonal matrice. Similarly we compute $(A_2(\phi^n)\phi^{n+1})_{i,j}$. The algorithm (1) describes the scheme of the proposed method.

Algorithm 1. Infinite Perimeter Area Fitting Selective Method Algorithm:
$\phi^k \leftarrow IPAFSM(\phi^{(0)}, \mathcal{A}, \mu, \nu, \beta, \alpha, \epsilon, maxit, tol)$.

Compute the distance function D (optional), the edge function g, the area of the polygon, f from equation (22), $\phi^{(1)} = \phi^{(0)}$;

for $iter = 1 : maxit$ **do**

Calculate $\phi^{(n)}$ from (24):

$\phi_l^{(n+1)} \leftarrow \frac{1}{2}\sum_{l=1}^{2}\ (\ I - 2\Delta t A_l(\phi^n))^{-1}\hat{\phi}^n$

If $\| \phi^{(n+1)} - \phi^{(n)} \| < tol$ or $iter > maxit$, set $\phi^{(k)} \leftarrow \phi^{(n-1)}$ Break;

else $\phi^{(n)} \leftarrow \phi^{(n-1)}$

update f from equation (22)

end for

---

5. EXPERIMENTAL RESULTS

In this section, we first argue the robustness of the proposed model for images with regular and oscillatory boundaries type of contours. The initial curve as the model suggests it is placed as near possible inside the given object by using the given markers to construct the zero level set (a polygon passing through the markers). Comparison with a similar one level set selective segmentation model, such as the Rada et al. [23] or Nguyen et al. [21] model has been shown. We perform experiments of our new method by using objects where oscillation boundaries are found. We compare the obtained results of the detected object of such boundaries with the dual-level set selective segmentation model with the infinite perimeter fitting term introduced by Rada et al. [24]. This comparison shows the speed advantage of the proposed method while keeping the same accuracy performance. Furthermore, we show the practical use of this model and its applications in fields such as medicine, where qualitative segmentations are of a great importance. Different size images, such as n = 128 (i.e. 128 × 128), n = 180 (i.e. 180 × 180), and n = 256 (i.e. 256 × 256) , n = 512 (i.e. 512 × 512) , has been used. The parameters k, γ, λ_1, λ_2, μ, μ_1, μ_2 and β used in the following tested experiments are fixed to the values k = 8, γ = 10, $\lambda_1 = \lambda_2$ = 100, μ = 1, μ_1 = 1, μ_2 = 0.0001, ϵ = 1, and $\beta = 10^{-6}$. Based on the quality that the AOS algorithm is unconditionally related to the time step size we use Δt = 1 in all our experiments and a relative residual of 10^{-2}.

Test Set 1 — Segmentation Accuracy and Its Comparison to Other Models

The first test set demonstrates the ability to properly segment objects with different shapes and intensity and then compare with Rada et al. [23] and Nguyen et al. [21]. Fig. 1 shows the segmentation result for two synthetic and two real-life images. The aimed object in the first image in Fig. 1 is a square placed nearby to an *L* shape geometrical object with the same intensity. The second image of this figure contains a geometrical object which has to be separated from the other geometrical objects. Furthermore, the object itself is not homogeneous inside the given geometrical markers (white background is found between the object itself). The third and the fourth images are knee and cell images with a high level of noise. From Fig. 1 we can easily notice that the proposed method correctly captured the aimed objects. We have to emphasise that the obtained results are similar to the previous work of Rada et al. [25, 23] overcoming the previous work of Gout et al. [12] and [3]. For briefness, we do not show the results obtained by the previous work of Rada et al. [25, 23, 24] but we note that both models give the same satisfactory results as shown in Fig. 1. For more details reader can refer to the results shown in [25, 23, 24] papers. Based on the same papers [25, 23], the results shown in Fig. 1 have the same results by Nguyen et al. [21] model given a proper initialization. In the following, we show test results where the proposed model performs better than Nguyen et al. [21] model. Comparison to Rada et al. [25, 23] work for such images is not shown as the obtained results are the same for such cases. Fig. 2 shows the comparison results between Rada et al. [25], Nguyen et al. model [21] and the proposed model for a Christmas tree in a pot and cell image in the first and the second row, respectively. We can easily notice successful results by Rada et al. [25] and the new model for a real-life image of a Christmas tree in a pot where the nearby pixels have different intensities in an oscillatory structure. The Nguyen et al. model [21] can sufficiently good capture the tree but fails to capture the whole pot due to semi-transparent boundaries. Nguyen et al. model [21] fails also to segment the nearby cell images, as shown in the second row due to the fact that the cells are of the same intensity and separated with one pixel between them. Fig. 2 show that Nguyen et al. [21] method cannot handle transparent or semi-transparent boundaries and noise. ,s figure we can clearly see that our method and Rada et al. [25] properly segment such cases.

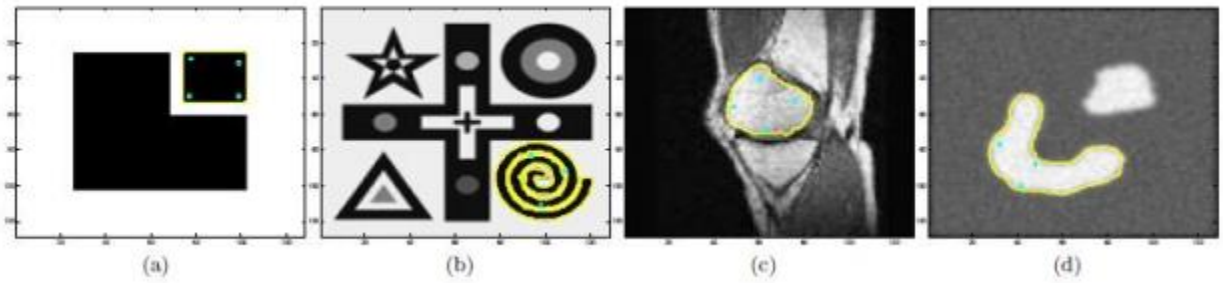

Figure 1. Test Set 1 – Successful segmentation of different images with the proposed method with given markers in blue color.

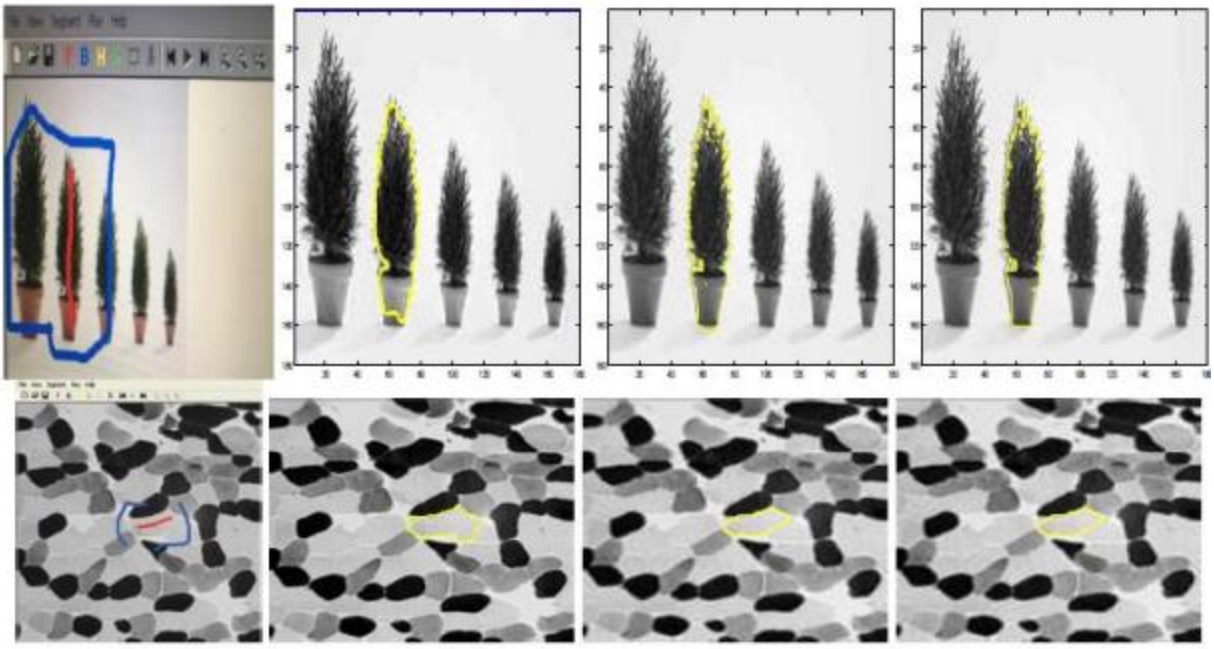

Figure 2. Test Set 1 – Comparison with Rada et al. [25] and Nguyen et al. model [21] for a Christmas tree in a pot and cell images in the first and the second row respectively.

Test Set 2 — Comparison with The Rada Et Al. [24] Model

The second set of experiments compares the proposed model with the infinite perimeter dual level set selective (IPDLSS) method [24] and show similar results for oscillatory boundaries by gaining a better performance speed. We demonstrate the ability of the new model to recognize specific objects with oscillatory boundaries while the proposed method has priority in terms of CPU time. In particular, we consider trees segmentation since the cornering effect of the model can be observed and the characteristic of these images is oscillatory boundaries.

Figs. 3, 4, and 5 show the compared results of the new model with the previous work of Rada et al. [23, 24]. Fig. 3 show the comparison of the model with Rada et al. [23]. Both models have the same speed of convergence and similar results. The speed of convergence is similar as both models run over one level set. In comparison with Rada et al. [24] model, we can notice that the proposed model performs accurate results for low-quality oscillatory data, similar to the previous work of Rada et al. [24] model and outperforms the Rada et al. [23] model as shown in Fig. 4. Looking into the segmentation results of those images, we can notice that the previous Rada et al. [23] model will lose some details between the tree's branches, see Fig. 5, taken from Fig. 4 left corner crop. We acknowledge that the parameter used for all the experiments are fixed as given at the beginning of this section. For better performance of the proposed method, the tuning of the parameters is required, such as the increase of the parameter k for better details in case of oscillatory boundary. In the following, we show the priority of the proposed method compared to the IPDLSS model [24] in terms of the speed of the convergence. IPDLSS model suffer from a slow convergence due to the fact that successively must update the global and local level sets. Table 1 shows clearly this fact. In this table, we compare the CPU time of new model with the old IPDLSS model [24] and find out that the new model is at least two times faster. In this table we show the results of 6 images but we acknowledge that similar results to Table 1 were obtained in all performed experiments without exceptions.

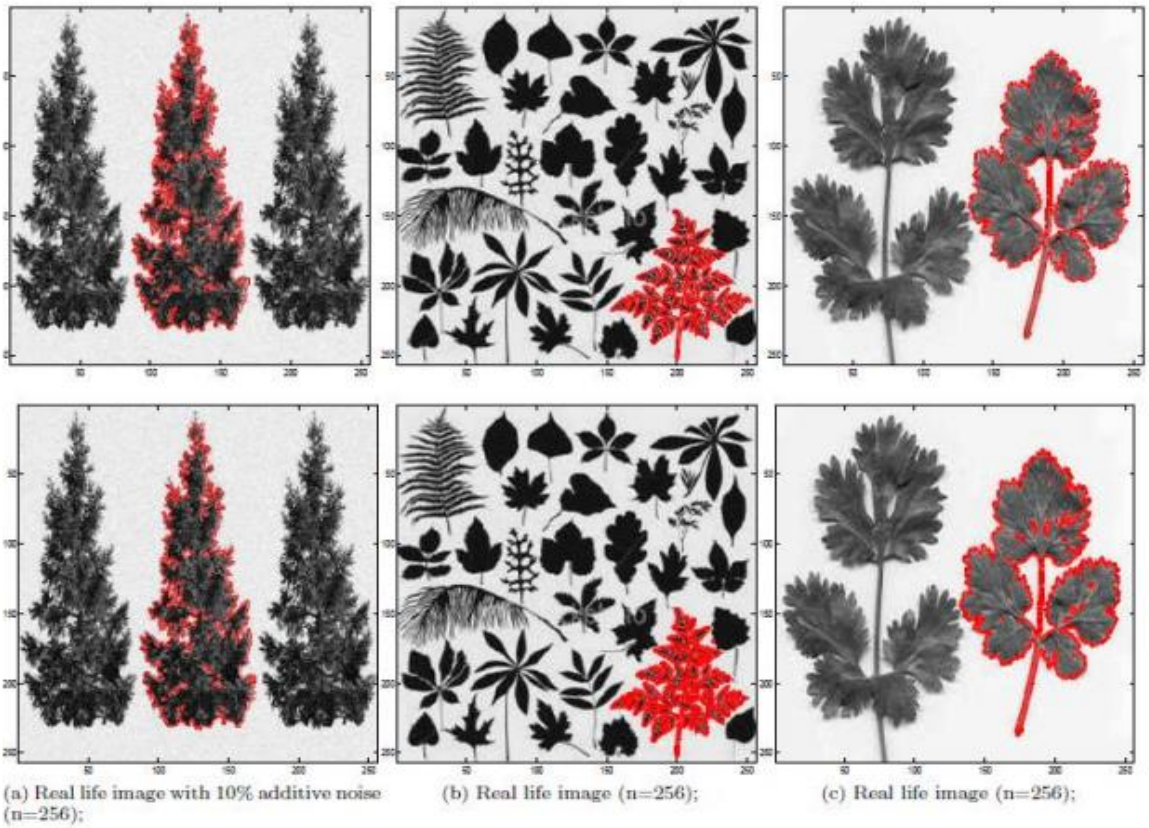

Figure 3. Segmentation results for Rada et al. [23, 24] models and the proposed selective segmentation model. The first column show the results obtained from Rada et al. [23] model, the second column the results obtained from Rada et al. [24] and the last column the obtained results with the new model.

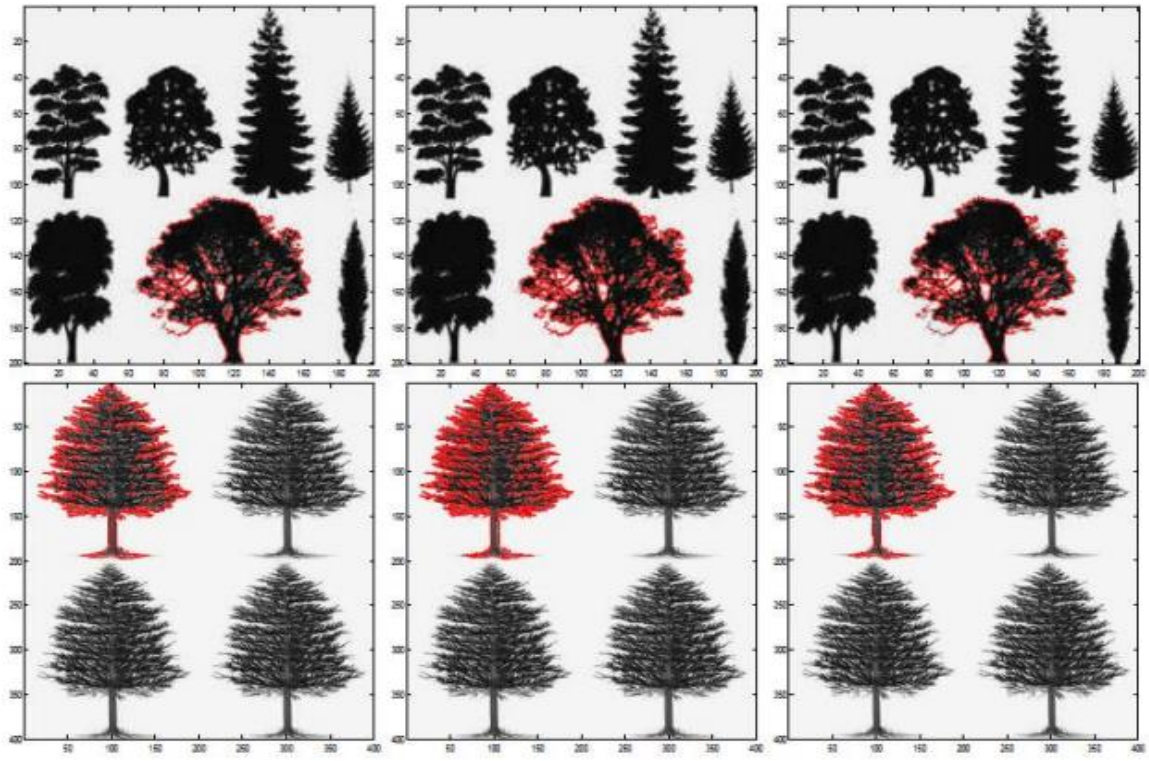

Figure 4. Segmentation results for Rada et al. [23, 24] models and the proposed selective segmentation model. The first column show the results obtained from Rada et al. [23] model, the second column the results obtained from Rada et al. [24] and the last column the obtained results with the new model.

Figure 5. Segmentation results for Rada et al. [23, 24] models and the proposed selective segmentation model. The first column show the results obtained from Rada et al. [23] model, the second column the results obtained from Rada et al. [24] and the last column the obtained results with the new model.

Table 1. Required CPU time for the proposed method and ist comparison to IPDLSS.

Figure	IPDLSS method CPU time	New method CPU time
Img. 1(256 × 256)	58.7938	16.3198
Img. 2(256 × 256)	49.5213	17.1265
Img. 3(256 × 256)	46.1250	17.7688
Img. 4(256 × 256)	35.4201	16.2090
Img. 5(256 × 256)	49.120	18.8890
Img. 6(256 × 256)	31.7601	17.8190

Test Set 3 — Useful Applications for Data Boundary Refinement

In this experiment, we show some useful applications where clearly the proposed model qualitatively refines the aimed boundaries. In this experiment, we use a public accessible PH2 dataset [31] consisting of 200 skin cancer images. The database collection was a collaboration between the Dermatology Service of Hospital Pedro Hispano in Matosinhos, Portugal, and The Universidade do Porto in Ecnico Lisboa. The database has two files: one of the files with the original image and another one consisting of lesion boundaries drown by the specialist of the field in a mechanical time-consuming process. We used this dataset to show that we can help the specialist correctly capturing and refining the lesion boundaries. Figs. 6 and 7 show the segmentation results of the proposed method compared with boundaries drawn by the specialist. In Fig. 6, we notice that there is a similar output of the drawn boundaries between the specialist, in the first row, and the proposed method, in the second row, whereas Fig. 7 show results where the proposed method can better distingue between healthy and non-healthy regions of the lesion. Such a result would be of help especially if laser-like techniques are used to burn the non-healthy cells.

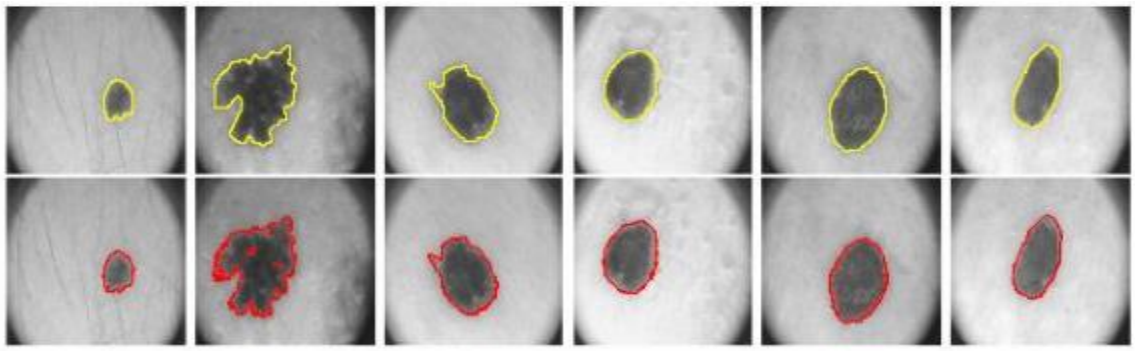

Figure 6. Segmentation results comparison for the original segmented lesion boundaries (made by a specialist) in the first row and the proposed method in the second row.

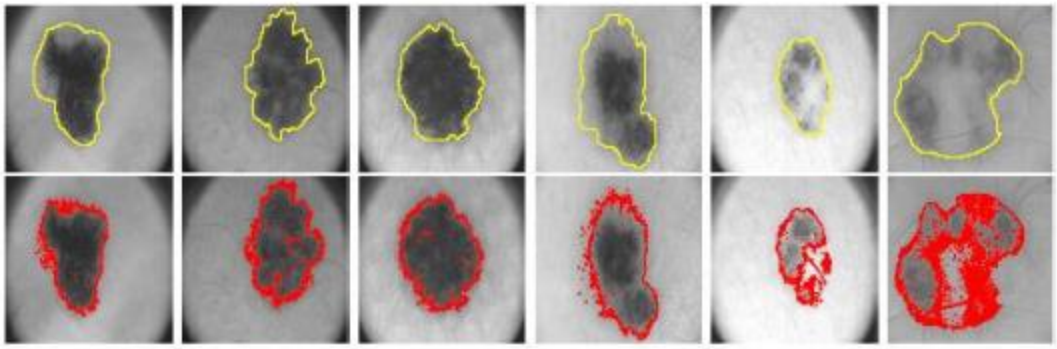

Figure 7. Segmentation results comparison for the original segmented lesion boundaries (made by a specialist) in the first row and the proposed method in the second row.

6. CONCLUSIONS

The presented variational selective segmentation model show reliable segmentation for the aimed object of interest with oscillatory boundaries. This model delivers similar results to old models, such as the Rada et al. model [24, 23] or better results for oscillatory boundaries compared to [25] and Nguyen et al. [21] model. The model improves the convergence speed of the Rada et al. [24] model by having the same accuracy for oscillatory boundaries objects. To indicate the significant contribution of this study we show some real-life applications using PH2 open-source dataset [31] with medical images where cancer segmentation is required. We can easily see through experiments that the proposed method has a really good quantitative segmentation.

7. REFERENCES

1. G. Aubert and P. Kornprobst. "Mathematical problems in image processing: Partial Differential Equations and the Calculus of Variations," Springer, 2001. ""

2. V. Badrinarayanan, A.Kendall, and R. Cipolla. "Segnet: A deep convolutional encoder-decoder architecture for image segmentation," CoRR., 2015.

3. N. Badshah and K. Chen. "Image selective segmentation under geometrical constraints using an active contour approach," Commun. Comput. Phys., 7(4):759–778, 2009.

4. M. Barchiesi, S. H. Kang, T. M. Le, M. Morini, and M. Ponsiglione. "A variational model for infinite perimeter segmentations based on lipschitz level set functions: Denoising while keeping finely oscillatory boundaries," Multiscale Modeling & Simulation, 8(5):1715–1741, 2010.

5. G. J. Brostow, J. Fauqueur, and R. Cipolla. "Semantic object classes in video: A high-definition ground truth database," Pattern Recogn. Lett., 2:88–97, 2009.

6. V. Caselles, R. Kimmel, and G. Sapiro. "Geodesic active contours. International Journal of Computer Vision," 22(1):61–79, 1997.

7. T. F. Chan and L. A. Vese. "Active contours without edges," 1998.

8. L. C. Chen, G. Papandreou, I. Kokkinos, K. Murphy, and A. L. Yuille. Deeplab: "Semantic image segmentation with deep convolutional nets, atrous convolution, and fully connected crfs, " IEEE Transactions on Pattern Analysis and Machine Intelligence, 40(4):834–848, 2018.

9. D. Comaniciu, P. Meer, and S. Member. "Mean shift: A robust approach toward feature space analysis" IEEE Transactions on Pattern Analysis and Machine Intelligence, 24:603–619, 2002.

10. S. Geman and D. Geman. "Stochastic relaxation, gibbs distributions and the bayesian restoration of images," IEEE Transactions on Pattern Analysis and Machine Intelligence, (6):721–741, November.

11. C. Gout, C. Le Guyader, and L. A. Vese, "Segmentation under geometrical consitions with geodesic active contour and interpolation using level set methods," Numerical Algorithms, 39:155–173, 2005.

12. C. Gout. "Viscosity solutions for geodesic active contour under geometrical conditions," International Journal of Computer Mathematics, 85(9):1375–1395, 2008.

13. C. Le Guyader and C. Gout. "Geodesic active contour under geometrical conditions theory and 3d applications," Numerical Algorithms, 48:105–133, 2008.

14. Steve Hanov. "Wavelets and edge detection," April 2006.

15. T. Lu, P. Neittaanmaki, and X. C. Tai. "A parallel splitting-up method for partial differential equations and its application to navier-stokes equations," RAIRO Mathematical Modelling and Numerical Analysis, 26(6):673–708, 1992.

16. J. Malik, Th. Leung, and J. Shi. "Contour and texture analysis for image segmentation," International Journal of Computer Vision, 43:7–27, 2001.

17. S. Mallat. "A wavelet tour of signal processing, "Academic Press, USA, 1998.

18. P. Morrow, S. McClean, and K. Saetzle. "Contour detection of labeled cellular structures from serial ultrathin electron microscopy sections using gac and prior analysis," IEEE Proceedings of IPTA, pages 1–7, 2008.

19. D. Mumford and J. Shah. "Optimal approximation by piecewise smooth functions and associated variational problems," Communications on Pure Applied Mathematics, 42:577–685, 1989.

20. D. Mumford and J. Shah. "Boundary detection by minimizing functionals," In IEEE Conference on Computer Vision and Pattern Recognition.

21. T. Nguyen, J. Cai, J. Zhang, and J. Zheng. "Robust interactive image segmentation using convex active contours," IEEE Transactions on Image Processing, 21:3734–3743, 2012.

22. S. Osher and J. A. Sethian. "Fronts propagating with curvature dependent speed: Algorithms based on hamilton-jacobi formulations," Journal of Computational Physics, 79(1):12–49, 1988.

23. Lavdie Rada and Ke Chen. "Improved selective segmentation model using one level-set," Journal of Algorithms & Computational Technology, 7(4):509–540, 2013.

24. Lavdie Rada and K. Chen. "On a variational model for selective image segmentation of features with infinite perimeter," volume 33, pages 253–272, 2013.

25. L. Rada and K. Chen. "A new variational model with dual level set functions for selective segmentation," CiCP, 12(1):261–283, 2012.

26. D. Sen and S. K. Pal. "Histogram thresholding using fuzzy and rough measures of association error," Image Processing, IEEE Transactions on, 18(4):879–888, 2009.

27. N. Valliammal and S. N. Geethalakshmi. "Performance analysis of various leaf boundary edge detection algorithms," In Proceedings of the 1st Amrita ACM-W Celebration on Women in Computing in India, A2CWiC '10, pages 34:1–34:6, 2010.

28. J. Weickert and G. Kühne. "Fast methods for implicit active contour," In N. Paragios S. Osher, editor, Geometric Level Set Methods in Imaging, Vision, and Graphics, pages 43–57. Springer New York, 1995.

29. J. Weickert, B.M. Romeny, and M.A. Viergever. "Efficient and reliable schemes for

nonlinear diffusion filtering," IEEE Transactions on Image Processing, 7(3):398–410, 1998.

30. Xiangrong Zhang, Feng Dong, G. Clapworthy, Youbing Zhao, and Licheng Jiao. "Semi-supervised tissue segmentation of 3d brain mr images," In Information Visualisation (IV), 2010 14th International Conference, pages 623 –628, 2010.

31. T. Mendonça, P. M. Ferreira, J. S. Marques, A. R. S. Marcal and J. Rozeira, "PH2 - A dermoscopic image database for research and benchmarking," 2013 35th Annual International Conference of the IEEE Engineering in Medicine and Biology Society (EMBC), 2013, pp. 5437-5440.

DOI: 10.38061/idunas.848233

IDUNAS | NATURAL & APPLIED SCIENCES JOURNAL | 2021 Vol. 4 No. 2 (32-37)

Predicting Purchase Interest of Online Shoppers Using Boosting Algorithms

Research Article

Başak Esin Köktürk Güzel[1*], Devrim Ünay[1*]

[1]Department of Electrical and Electronics Engineering, Izmir Democracy University, İzmir, Turkey.

Author E-mails
basakesin@zoidata.com
devrim.unay@idu.edu.tr

*Correspondance to: Başak Esin Köktürk Güzel, Department of Electrical and Electronics Engineering, Izmir Democracy University, İzmir, Turkey.
DOI: 10.38061/idunas.848233

Received: 28.12.2020; Accepted: 30.06.2021

Abstract

Data driven marketing is becoming more and more vital for businesses day-by-day. Understanding customer behavior has the potential to decrease marketing costs as well as increase sales both in conventional marketing and online marketing. Since online users can access information faster, prices have become more competitive and customer behavior analysis has become more important. The purpose of this study is to predict the purchase interest of the users in an e-commerce web page by using the user session data such as pageview, duration etc. To this aim we used clickstream data for an e-commerce web page which is publicly available. Since only 16.5 percent of the sessions are completed with purchase in the dataset, increasing true positive rates rather than accuracy is more important. To this aim, we have explored the performance of boosting algorithms on the dataset and compared to those of state-of-the-art methods that were previously applied on the same dataset. Results show that boosting algorithms have better performance for identification of the sessions that end with a purchase.
Keywords: Online shopping intention prediction, boosting algorithms, adaboost, gradient boosting, extreme gradient boosting.

1. INTRODUCTION

Online shopping has experienced a rapid growth in recent years, as it offers solutions to 24/7 service needs, is less costly and has a wide range of products.

The global Coronavirus outbreak has had a major impact on societies around the world as well as brands and retailers including the way of shopping. The new conditions, caused by pandemic, have given rise to many brick-and-mortar stores temporarily closed, and thus people are going online to buy goods and services. In the first and second quarter of 2020, revenue of e-retailers have grown dramatically from 11.8% up to 16.1% of total retail sales in the US (Statistica, 2020). This situation has increased the competition

among electronic commerce (e-commerce) sites. During shopping, online shoppers can not only compare the price of the product they are interested in, but also decide based on the reliability and customer satisfaction of each site. Therefore, it is important to measure the purchasing tendencies of online buyers, to make improvements or to reveal the causes of operations that enable and/or inhibit purchasing.

Traditional retail stores can target their potential customers through conventional ways. But it is not possible to identify potential customers by e-commerce sites. However they are able to predict potential buyers by the help of collected data. The decision-making with these predictions can increase both the experience of the users and the recycling rates of sales. Several studies have been conducted to evaluate parameters that determine the online shopping trends of users.

Predicting the online shoppers purchase interest by observing their behavior in the considered online platform (usually by analyzing their behavior in the shopping website) is an interesting topic because if you can predict whether a user will make a purchase or not you got a massive economical information. Some of the related research focused on minimizing shopping cart abandonment by predicting user behavior in real-time (Awad & Khalil (2012), Budnikas (2015), Fernandes (2015)) while others aimed at segmenting customers according to their navigational patterns (Carmona et.al. (2012), Kau et.al. (2003), Moe (2003)). Sakar et al. (2019) compared the performances of different models such as Random Forests (RF), Support Vector Machines (SVM) and Multilayer Perceptron (MLP), and found that the accuracy and f-1 score of the MLP model were significantly higher than those of the RF and SVM models.

This study was designed to estimate whether a user section will end with a sale or not. By predicting purchase interest of a user, marketing campaigns can design according to the user and this provides to increase the conversion rate of the campaign. To this aim, we have applied boosting classifiers on the "Online Shoppers Purchasing Intention Dataset" which is published by Sakar et.al. (2019) and compared the performance of three boosting classifiers.

This paper is structured as follows. Section 2 describes the boosting methods, while Section 3 introduces the dataset used in this study. Section 4 presents the results of the boosting methods for prediction of users' purchase interest in e-commerce web pages. Section 5 concludes the paper by detailed discussions on the results and the potential future works.

2. METHODS

"Boosting" refers to creating a strong learner from the weak learners in machine learning applications. The boosting algorithms learn from the mistakes of weak learners and construct a potentially more robust and accurate classifier. They have an iterative approach where each learner focuses on correcting the mistakes of the previous learners. Adaboost and Gradient Boosting are the most popular boosting classifiers (Köktürk Güzel & Önder ,2018). In recent years, Extreme Boosting got attention in almost all data mining competitions because of its high classification accuracy and low computational cost. In this study we have used three types of boosting algorithms to predict buyers intention in online shopping web pages. Following sections introduce background information on these algorithms.

Adaboost

Adaboost assigns same weights to all samples in the beginning, but then updates the sample weights sequentially by giving higher weights to misclassified samples in the later iterations (Figure 1). To create a strong classifier, the algorithm takes the weighted sum of each learner output (Freund & Schapire (1995)).

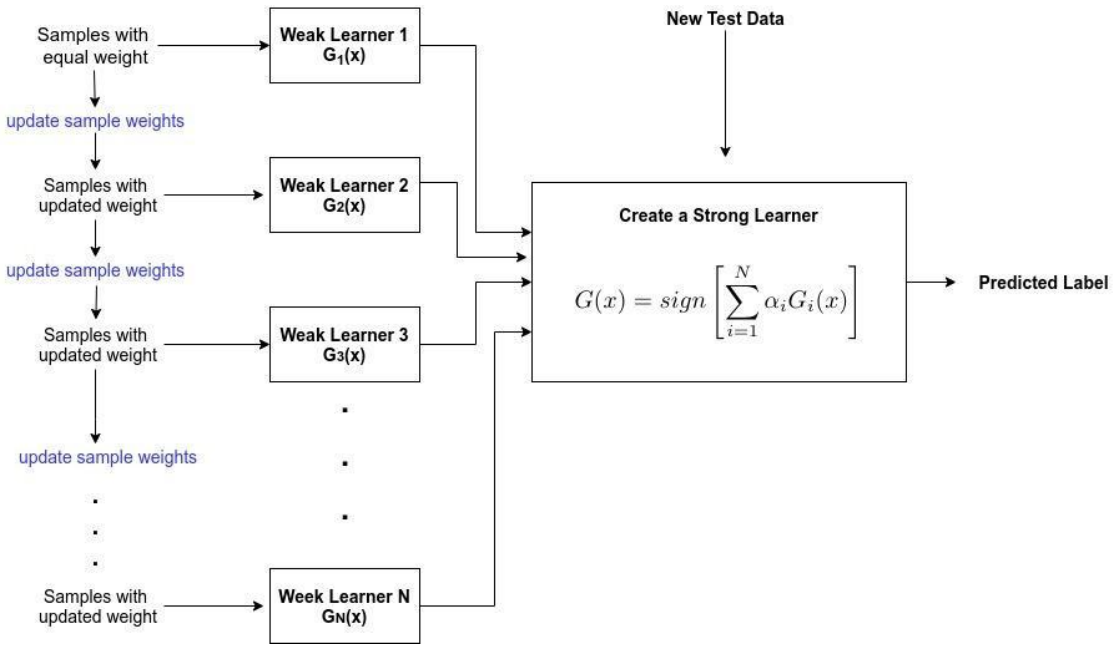

Figure 1. The schematic of the Adaboost algorithm.

Gradient Boosting

Like Adaboost, the Gradient Boosting algorithm also combines weak learners into a single strong learner in an iterative fashion (Figure 2). However, the gradient boosting algorithm trains learners with the error of the previous learner. Therefore it fits a function on the residual of the previous learner and attempts to correct this error (Friedman, 2001).

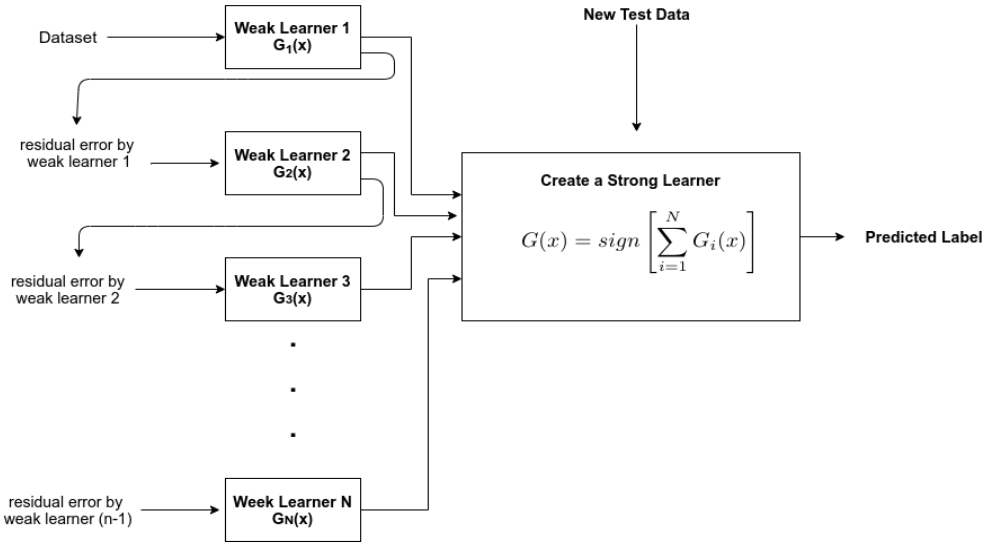

Figure 2. The schematic of the Gradient Boosting algorithm.

Extreme Gradient Boosting

Extreme Gradient Boosting (XGBoost) basically has a gradient boosting framework with more powerful features such as parallel computing, handling missing values, and regularization to avoid overfitting or bias. In other words, XGBoost is an implementation of the gradient boosting algorithm where it gets its power from system optimization and algorithmic enhancements. The XGBoost algorithm solves

the optimization problem by determining the step size and step direction in the same time (Chen and Guestrin 2016).

In the next section, we briefly describe our dataset and the features which we used in this study.

3. DATASET

The dataset has 12330 sessions (each belonging to different unique users) recorded with attributes related to web page analytics in a 1-year period. This 1-year duration has been selected according to certain criteria to avoid any tendency to a specific campaign, special day, user profile, or period. Only 16.5 percent of the samples have positive labels which mean the sessions ended with purchases (Sakar et al. 2019). The dataset, publicly available in the UCI Machine Learning Repository platform, has attributes listed with their descriptions in Table1.

Table 1. Names and Descriptions of the Attributes present in the Dataset (Sakar et al. 2019).

Attribute Name	**Attribute Description**
Administrative	Number of pages visited by the visitor about account management
Administrative_Duration	Total amount of time (in seconds) spent by the visitor on account management related pages
Informational	Number of pages visited by the visitor about Web site, communication, and address information of the shopping site
Informational_Duration	Total amount of time (in seconds) spent by the visitor on informational pages
ProductRelated	Number of pages visited by visitor about product related pages
ProductRelated_Duration	Total amount of time (in seconds) spent by the visitor on product related pages
BounceRates	Average bounce rate value of the pages visited by the visitor
ExitRates	Average exit rate value of the pages visited by the visitor
PageValues	Average page value of the pages visited by the visitor
SpecialDay	Closeness of the site visiting time to a special day
Month	Month value of the visit date
OperatingSystems	Operating system of the visitor
Browser	Browser of the visitor
Region	Geographic region from which the session has been started by the visitor
TrafficType	Traffic source by which the visitor has arrived at the Web site (e.g., banner, SMS, direct)
VisitorType	Visitor type as “New Visitor,” “Returning Visitor,” and “Other”
Weekend	Boolean value indicating whether the date of the visit is weekend
Revenue	Class label indicating whether the visit has been finalized with a transaction

In the next section we presented the results of classifiers on this dataset.

4. RESULTS

We have used the boosting classifiers to predict the result of a session (whether ended with a purchase or not) in an online shopping website. Note that, in this problem the number of positive samples is 16% of all the samples. So, estimating true positives are more challenging. If we predict all samples as negative our accuracy will be ~84% so to understand the performance of a classifier we also listed f1 measures which is a harmonic mean of precision and recall. Table 2 reports the performances of the algorithms on the cross-validated training data via accuracy and f1 measure scores that are computed using the corresponding confusion matrices.

Table 2. Cross-validation scores of the boosting algorithms on training data reported as mean (standard deviation).

	Adaboost	Gradient Boosting	XGBoost
Accuracy	0.892873 (0.014213)	0.904614 (0.013199)	**0.906672 (0.014580)**
f1-measure	0.622838 (0.050687)	0.659376 (0.042769)	**0.664804 (0.051171)**

Table 3. Test scores of the boosting algorithms.

	Adaboost	Gradient Boosting	XGBoost
True Positive Rate	0.541864	**0.586098**	0.578199
True Negative Rate	0.950815	**0.957509**	0.956636
Accuracy	0.887196	**0.899730**	0.897764
f1-measure	0.599127	**0.645217**	0.637631

Since the results show that performances of the algorithms are very close, we have applied t-test on the prediction results in a pairwise manner. The p-value between the predictions of XGBoost and AdaBoost classifiers is 0.043, which shows that XGBoost classifier has significantly better performance than Adaboost classifier for predicting the shoppers' purchase intention. However, when we calculate the p-value between predictions of XGboost classifier and Gradient Boosting classifier, we obtain a p-value of 0.19 which means that the performances of the classifiers are statistically indifferent.

Python programming language was used in our implementation and all source codes of this study are publicly available at Github page13 in order to allow for reproducibility of our results.

5. CONCLUSION

In this paper, we have presented a comparative study on the classification performances of boosting algorithms for predicting the shopping intention. Previously, Sakar et. al. (2019) published the classification results of multilayer perceptron and support vector machines on the same dataset. Here, we demonstrated that performance of boosting algorithms to identify positive samples is better than the state-of-the-art. We have achieved an average f1 measure of 0.664 using the XGBoost algorithm. We have obtained our results

on an open database and made our implementation publicly available to help further the research in this domain.

Our results support the argument that shopping intention from a clickstream data can be predicted using boosting methods. The technology discussed here is working as an offline classifier, however it has potential in real-time prediction problems. Designing a system that predicts the purchase interest in an online session has significant economic gain for e-retailers. Towards that aim, further research can be performed with the help of marketing experts to exploit domain knowledge.

6. REFERENCES

1. Awad, M. A., & Khalil, I. (2012). Prediction of user's web-browsing behavior: Application of markov model. IEEE Transactions on Systems, Man, and Cybernetics, Part B (Cybernetics), 42(4), 1131-1142.

2. Budnikas, G. (2015). Computerised recommendations on e-transaction finalisation by means of machine learning. Statistics in Transition. New Series, 16(2), 309-322.

3. Carmona, C. J., Ramírez-Gallego, S., Torres, F., Bernal, E., del Jesus, M. J., & García, S. (2012). Web usage mining to improve the design of an e-commerce website: OrOliveSur. com. Expert Systems with Applications, 39(12), 11243-11249.

4. Chen, T., & Guestrin, C. (2016, August). Xgboost: A scalable tree boosting system. In Proceedings of the 22nd acm sigkdd international conference on knowledge discovery and data mining (pp. 785-794).

5. Fernandes RF, Teixeira CM (2015) Using clickstream data to analyze online purchase intentions. Master's thesis, University of Porto.

6. Freund, Y., & Schapire, R. E. (1997). A decision-theoretic generalization of on-line learning and an application to boosting. Journal of computer and system sciences, 55(1), 119-139.

7. Friedman, J. H. (2001). Greedy function approximation: a gradient boosting machine. Annals of statistics, 1189-1232.

8. Kau, A. K., Tang, Y. E., & Ghose, S. (2003). Typology of online shoppers. Journal of consumer marketing, 20(2), 139-156.

9. Köktürk Güzel, B. E., & Önder, D. (2018, May). Performance comparision of boosting classifiers on breast termography images. In 2018 26th Signal Processing and Communications Applications Conference (SIU) (pp. 1-4). IEEE.

10. Moe, W. W. (2003). Buying, searching, or browsing: Differentiating between online shoppers using in-store navigational clickstream. Journal of consumer psychology, 13(1-2), 29-39.

11. Sakar, C. O., Polat, S. O., Katircioglu, M., & Kastro, Y. (2019). Real-time prediction of online shoppers' purchasing intention using multilayer perceptron and LSTM recurrent neural networks. Neural Computing and Applications, 31(10), 6893-6908.

12. Statistica 2020 – www.statista.com/statistics/187439/share-of-e-commerce-sales-in-total-us-retail-sales-in-2010/

13. https://github.com/basakesin

DOI: 10.38061/idunas.850198

IDUNAS	NATURAL & APPLIED SCIENCES JOURNAL	2021 Vol. 4 No. 2 (38-52)

BabyTube Ruby on Rails Based Automatic Video and Image Tagging Application

Research Article

Leyla Kapi Kurtul[1*], Meriç Çetin[2*]

[1]Ruby on Rails Developer at YFU-Deutschland Oberaltenallee 6, 22081 Hamburg, Germany.

[2]Department of Computer Engineering, Pamukkale University, Kınıklı Campus, Denizli, Turkey.

Author E-mails
leylakapi@gmail.com
mcetin@pau.edu.tr

*Correspondance to: Leyla Kapi Kurtul, Ruby on Rails Developer at YFU-Deutschland Oberaltenallee 6, 22081 Hamburg, Germany.
DOI: 10.38061/idunas.850198

Received: 30.12.2020; Accepted: 09.07.2021

Abstract

The importance of technology in our lives is increasing day by day. The ability of people to keep up with developing technology is related to their correct and effective use of technology. Although positive contributions are detected in the use of technology and internet interactions, especially for people in early childhood, negative effects may be observed depending on the duration of exposure. For instance, thanks to the opportunities provided by technology, people in early childhood contribute to their language, cognitive or psycho-motor development. In addition to these positive features, the widespread use of technological tools has extremely harmful effects on the environment and human health. According to pedagogues, children between the ages of 2 and 12 are consumers of image/video contents on websites. When the contents watched/seen is not under the supervision of the parents, the subliminal message to be given may affect the development of children negatively. For the stated reasons, it is obvious that the videos/images uploaded in the web environment should be filtered and a content editor is required. In this paper, a software was developed to prevent the negative aspects of technological interactions (computer, tablet, phone, internet) of people in early childhood. This developed software automatically tags the contents in the web environment with Ruby on Rails based video and image processing. Using automatic content tagging, personal content control can be performed by providing systematic control over the web 7/24. More than 90% accuracy performance was achieved thanks to the power of Ruby and the Clarifai service, which is based on computer vision methods. It is thought that this approach will contribute to strengthening the social communication of people in the early childhood and developing their imaginations. The accuracy of the Ruby on Rails based video and image processing application has been tested with various machine learning techniques in this study. Therefore, it can be said that the developed software will pave the way for children to be mentally, physically and sensually healthier. In this way, it will be possible

to prevent various diseases (dyslexia, asperger syndrome, autism), which have increased in recent years and have been stated by some sources as technology based.
Keywords: Ruby on Rails, Clarifai, video and image tagging, content categorization, web application.

1. INTRODUCTION

The early childhood covering the period from birth to primary school age is very important for child development and education (Kaçar and Doğan, 2007). At these periods, which are thought to be critical for child development, the individual acquires basic knowledge, skills and habits (Çevik et al., 2017). Their dream worlds and perceptions are highly developed, and at the same time they are active, curious and investigative (Şahin and Akman, 2018). The education should not be left to chance at the early childhood, and it should be carried out systematically.

Technology has been an indispensable part of human life by shaping the environment since its existence (Sayan, 2016, Ergüney, 2017). The importance of technology in our lives is increasing day by day. The ability of people to keep up with developing technology is related to their correct and effective use of technology. Besides, it should not be forgotten that technological devices and internet usage are just tool for us. Although positive contributions are detected in the use of technology and internet interactions, especially for people in early childhood, negative effects may also be observed depending on the duration of exposure (Güngör, 2014, Aral et al., 2018). For instance, thanks to the opportunities provided by technology, people in early childhood contribute to their language, cognitive or psycho-motor development.

It has been stated that the use of technology in early childhood supports abilities such as imagination, different and analytical thinking, problem solving, and creativity (Dilekmen and Bozan, 2014, Akgündüz and Akpınar, 2018). In addition to these positive features, the widespread use of technological tools has extremely harmful effects on the environment and human health. There are many studies in the literature investigating the effect of technology usage on family communication. In these studies, it has even been stated that excessive usage of technology may cause the factors that hold the family together to disappear. The members of family rely on technology to increase efficiency in their home, school, business and social life (Claxton et al., 2016). Children as well as adults in the family are exposed to the use of technology, voluntarily or unintentionally. Some studies indicate that an average of 7.5 hours of technological device and / or internet use per day in early childhood. It is observed that the mental development of the children is negatively affected due to the usage of technological devices such as tablets, PCs, phones or internet. According to pedagogues, children between the ages of 2 and 12 are consumers of image/video contents on websites. Although the content encountered is instructive, the subliminal message may adversely affect child development. When the contents watched/seen is not under the supervision of the parents, even worse results can occur. For the stated reasons, it is obvious that the videos/images uploaded in the web environment should be filtered and a content editor is required.

Automatic identification of media contents such as images or videos is very important for their analysis. Although low-level diagnostic processes were used in previous years, many advanced studies have been conducted in terms of content characterization, emotion recognition or interactive content generation in recent years (Kanishcheva and Sharonova, 2018, Li et al., 2019). Most of these studies are based on deep learning networks, image processing techniques and various artificial intelligence methods. In this paper, a software was developed to prevent the negative aspects of technological interactions (computer, tablet, phone, internet) of people in early childhood (Kapi, 2019). This developed software automatically tags the contents in the web environment with Ruby on Rails based video and image processing. Using automatic content tagging, personal content control can be performed by providing systematic control over the web 7/24. It is thought that this approach will contribute to strengthening the social communication of people in

the early childhood and developing their imaginations. The accuracy of the Ruby on Rails based video and image processing application has been tested with various machine learning techniques in this study. Therefore, it can be said that the developed software will pave the way for children to be mentally, physically and sensually healthier. In this way, it will be possible to prevent various diseases (dyslexia, asperger syndrome, autism), which have increased in recent years and have been stated by some sources as technology-based.

2. WHAT IS BABYTUBE?

The starting point of this study is based on the impact of technology on child health. BabyTube is a video sharing platform controlled 24/7 by systematic controls. Thanks to this application, internet interactions of individuals in early childhood are controlled and filtering of negative content is guaranteed. BabyTube, which is basically developed with Ruby on Rails, works in integration with a wide variety of technologies. In the future, the videos are planned to be stored in databases on Amazon Web Service (AWS) in the cloud. In this way, it is thought that this non-profit application can take advantage of the numerous features of AWS for free. The working principle of BabyTube is as follows:

- The contents uploaded to the system by the user are taken into the video/image processing process.
- The tags are created for the relevant video/image.
- Thanks to the control mechanism, the videos are filtered according to the produced tags.
- The videos are automatically separated according to the profile-based keywords determined by the parents as a result of the filtering.
- Finally, the related content is made accessible to everyone by the administrator.

Using the BabyTube application, parents get information about the content that their children access and give them freedom in their content choices. In addition, BabyTube application monitors and analyzes the user's movements thanks to AI (Artifical Intelligence) based system features.

3. BABYTUBE CODING AND WORKING STRUCTURE

In that section talking about technologies which are used in BabyTube, coding structure, and working style of application. BabyTube coding and working structure are gathered under three main headings and detailed.

Technologies Which Are Used

The current technologies used in BabyTube application are as follows:

- HTML
- HAML
- CSS
- SASS
- Bootstrap
- Coffescript
- PostgreSQL
- Ruby
- Ruby on Rails
- NodeJS

- Clarifai API
- Yandex Metrica

Ruby is an open-source free software developed by Yukihiro Matsumoto (Flanagan, 2008). Ruby on Rails is a web framework developed by David Heinemeier Hansson (DHH) and written in the Ruby programming language (Bächle and Kirchberg, 2007). Ruby on Rails structure, which is generally used in web-based applications, contains all the components that applications need (Ruby on Rails Software, 2021). The strength of the Rails framework is that it is open source. In this way, it provides great flexibility and freedom to developers.

Coding Structure

Tables and table relationships are shown in Figure 1 for developed BabyTube Ruby on Rails application. Rails model structure is that provides the relationship between data in database and packages. There are not only relationships but also connections in the structure. The explanation of these connections over the video and tag relationship in the system is shown in Figure 2. Besides the video model, the user model has also been added. The relationship between user and video is shown in Figure 3. There is no doubt these facilities which are in the model structure increase use of Ruby on Rails. In Figure 4, a representation from the model class is given. User ownership is added with the 'has_many' relationship in the user model. In this way, the structure that enables the user to access videos and tags and the relationships in the database are added to the model's side. The use of the Rails web framework also increases thanks to the convenience in the model structure, such as the developer's application without open the database from within the model.

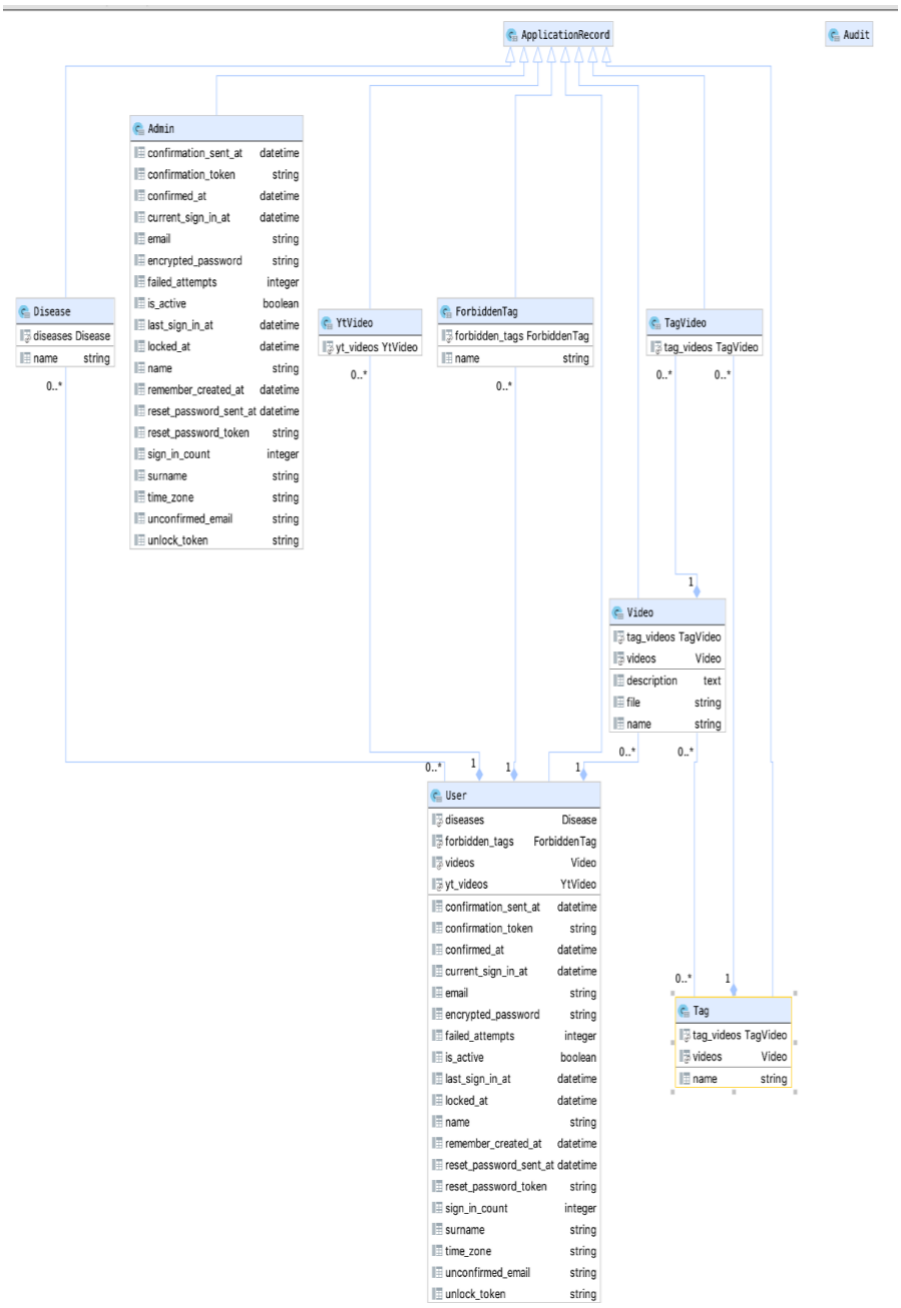

Figure 1. BabyTube database schema.

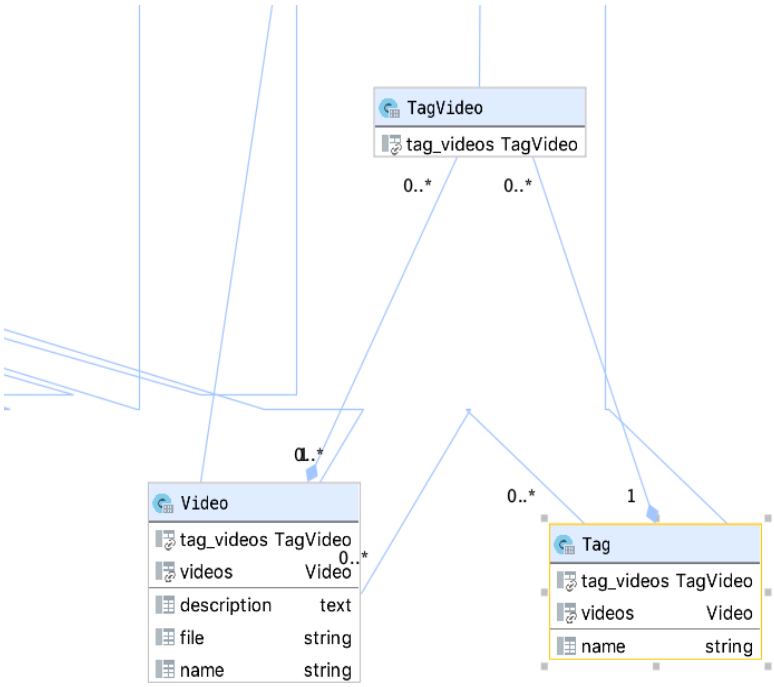

Figure 2. Database representation of the relationship structure between video and tag.

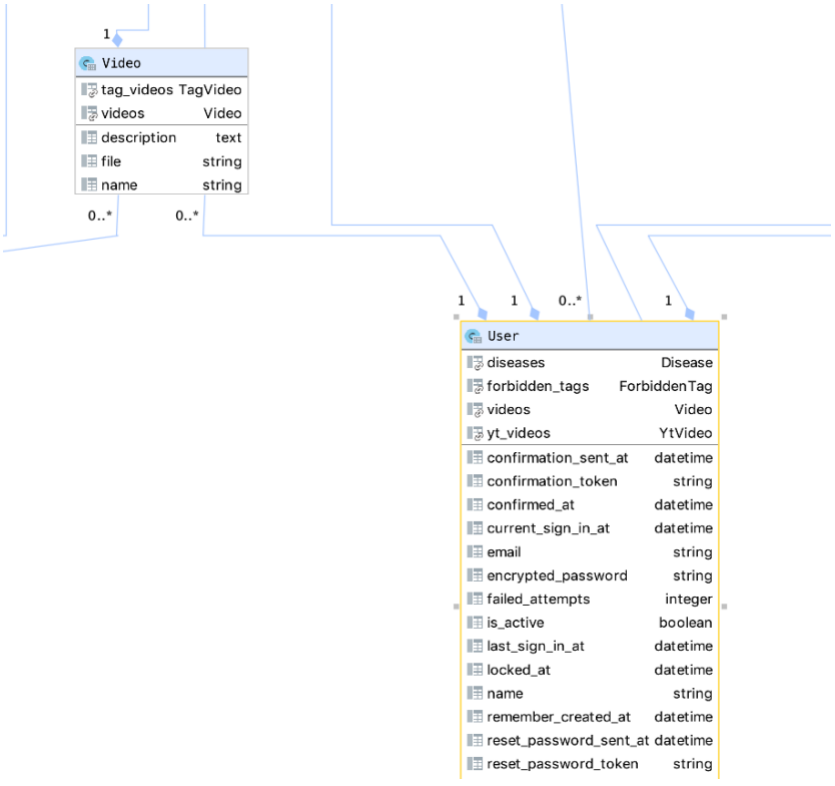

Figure 3. Database representation of the relationship structure between video and tag.

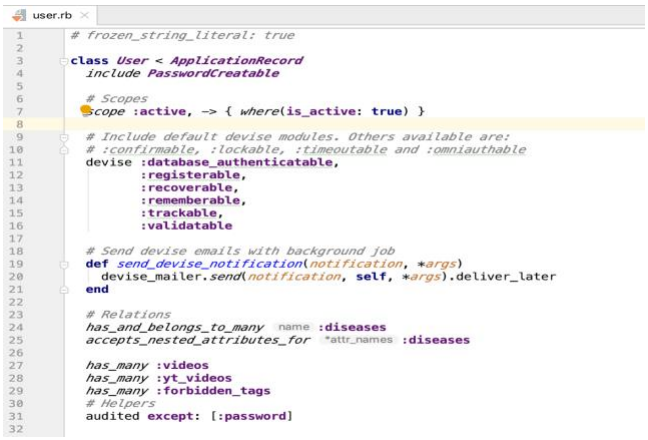

Figure 4. The representation of database from model class.

Controller Structure

Model-View-Controller (MVC) is an important framework that includes a View-Controller (VC) framework. In MVC, Action Controller handles the user interaction and carries out the control task of the structure. Basically, session management, template creating and redirecting. Action View is responsible for template management and provides control of the views displayed on the screen. This layer has many technologies supports. The last part is Action Dispatch. It sends the relevant request to the relevant links according to the structure of the requests. The structure that should be executed on the terminal for the control structure in the application is the "rails g controller controller_name" command. By using "rails generate controller video" command in terminal, the video control structure is added as shown in Figure 5.

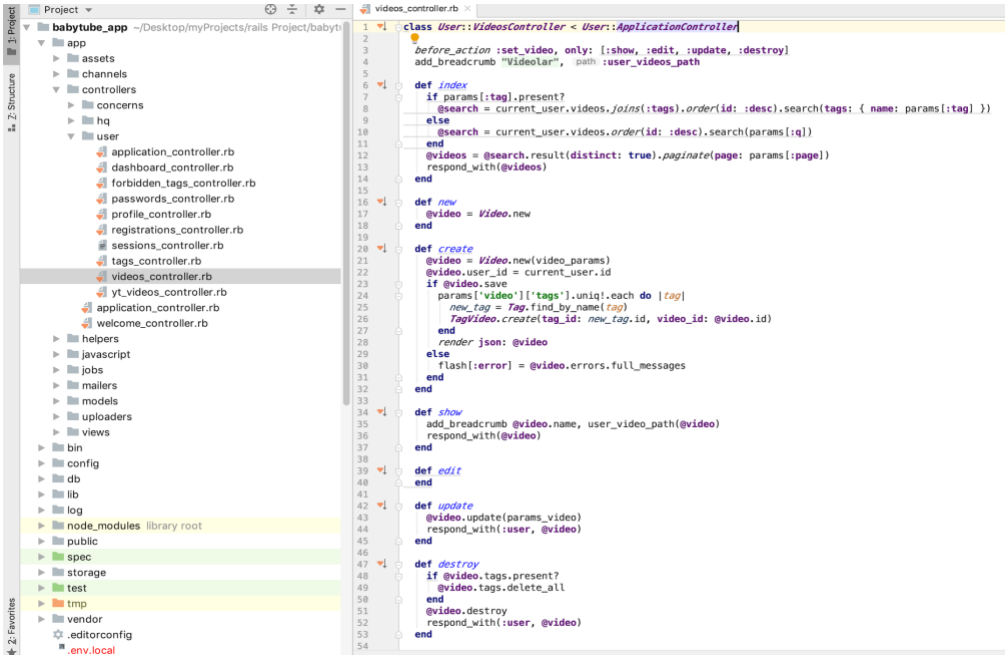

Figure 5. Video control structure.

Router Configuration

The router in Rails is a router module that recognizes browser URLs and sends them to the requested controller actions. When a URL is entered into the domain, the Rails router structure knows which controller

and action will handle the URL. Routers also work with incoming control structures and show the outputs to the end user. Figure 6 shows the Rails route structure schematically.

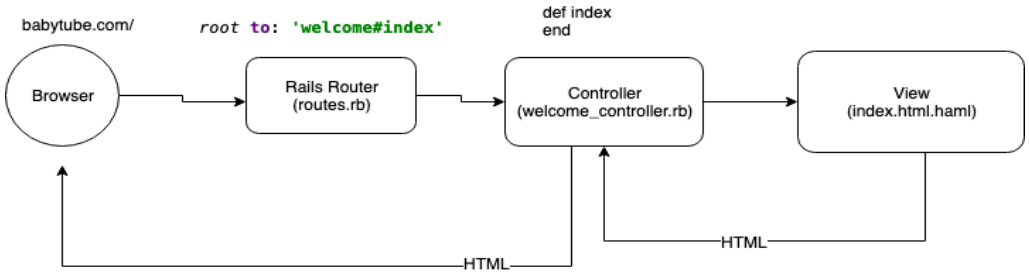

Figure 6. Rails route structure.

Gems Structure

A "Gemfile" is a file used in Ruby programs to define "gem" dependencies. A "Gem" is a collection of code made up of many Ruby files that can be used later. The "Gemfile" file should always be in the root directory of the project. In general, Ruby on Rails can add desired features very easily with its "Gem" structure.

Some of the "Gem" structures of Ruby on Rails (ROR) application can be summarized as follows:

i) The "Devise Gem" is one of the most popular libraries for authenticating in Rails applications.
ii) The "Simple-form Gem" is a library that is used to improve the form structures in the system and make the forms perfect with powerful components. Thanks to the "Simple-form Gem" structure, the code quality increases, and a cleaner code structure is offered.
iii) The "YT Gem" provides integration of YouTube videos to the system. This feature not only brings the videos but also the features of the videos.
iv) By using "Carrierwave gem", image and video structure is added to the system. In this way, video and image upload is provided in a very easy and practical way. In addition, it provides the opportunity to store the files in the desired format and size, so that the same file can be displayed, stored and worked on in different formats.

Working Structure and Clarifai API

Clarifai service is a popular third-party service that makes inferences from images, videos and text using computer vision and natural language processing in a one integrated AI Computer Vision platform (Clarifai, Technology, 2021). Clarifai is a machine learning method which utilizes CNN-Convolutional Neural Networks and DNN-Deep Neural Networks to analysis processes. Machine CORE (Clarifai Object Recognition Engine) is behind this learning method, thus, it is possible to test millions of images with this system. A comparison of Clarifai with leading API providers is shown in Table 1.

Table 1. Comparing the features of Clarifai and other tools

Features	Amazon	Google	Clarifai	Microsoft
Image tagging	Yes	Yes	Yes	Yes
Video tagging	Yes	Yes	Yes	Yes
Emotion detection	Yes	Yes	Yes	Yes
Logo detection	Yes	Yes	Yes	Yes
NSFW tagging	Yes	Yes	Yes	Yes
Dominant color detection	Yes	Yes	Yes	Yes
Feedback API	No	Yes	Yes	No
Price (per 1000 image)	1$	1.50$	1.20$	1.50$
Free request right	5000/Month	1000/Month	5000/Month	5000/Month
Image size limit	5Mb/Image	20Mb/Image	Undefined	4Mb/Image

Clarifai API, which can work in integration with many programming languages, is a more effective and easy service compared to its equivalents. An example of image analysis with Clarifai API is as: In web application, 100 default requests were made to the Clarifai service for both tested images. The obtained simulation results were published as good, good and bad (irrelevant). The images presented in Figure 7 were tested by Clarifai service with colored pages.

Figure 7. Croissant and Main Coon Cat images.

In 100 requests for Croissant: The best result was found at 98% level as "Croissant". Good level 96% "Bread", 93% "Dough" and 87% "Sugar" returned. At the worst level, 83% returned an irrelevant label as “Cooling”. 100 requests in the Main Coon Cat Image: As 100% "Cat" at the best level returned. At a good level 99% "Cute", 96% "Purebred" and 94% "Furry" returned. It returned a tag that was 94% “Young” at a poor level. To explain in detail, the calls for croissant painting the croissant returned at 98, and this is the best match.

How Application is Working?

In the application, the user uploads the desired videos to the system after logging in to the page. As a result of the application, the tags in the video analysed are obtained. These tags are used later for search and filter operations. In addition, when the "video id" information is given as input, videos suitable for the content can be presented to the user via the "Youtube" application.

After register or signed into the application, by using the "New Video" button, the mp4 file can be uploaded to the system and a new video can be added for analysis. While the video is uploaded to the system, NodeJS starts to analyze the video. Afterwards, with a "post" request, the tags are saved in the controller structure. The tags returned as a result of the "POST" request are shown in Figure 8. A different "post" request is sent to save the returned tags to the database.

As an example, Figure 8 shows the returned tags and accuracy percentages for a 5-second video (https://www.youtube.com/watch?v=EngW7tLk6R8) added to the application. The application returns many tags as a result of video analysis and these tags are listed as those with an accuracy value greater than "0.90".

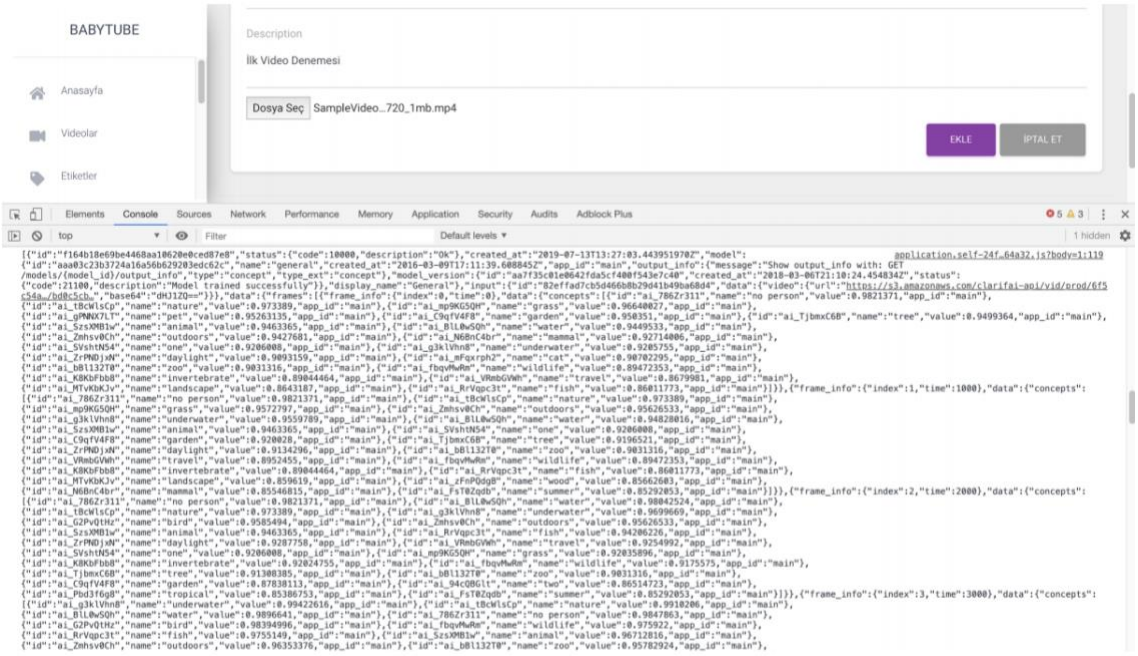

Figure 8. Tags that return at the end of the analysis after video is uploaded.

A different "POST" request is sent to save the returned tags to the database. The result of this post request is shown in Figure 9. Using this application, a comparison can be made from the tags returned from the uploaded and analysed videos. Additionally, videos containing user-specified prohibited words can be blocked from uploading. For example, the forbidden word is "tree". The code block required for content blocking is shown in Figure 10.

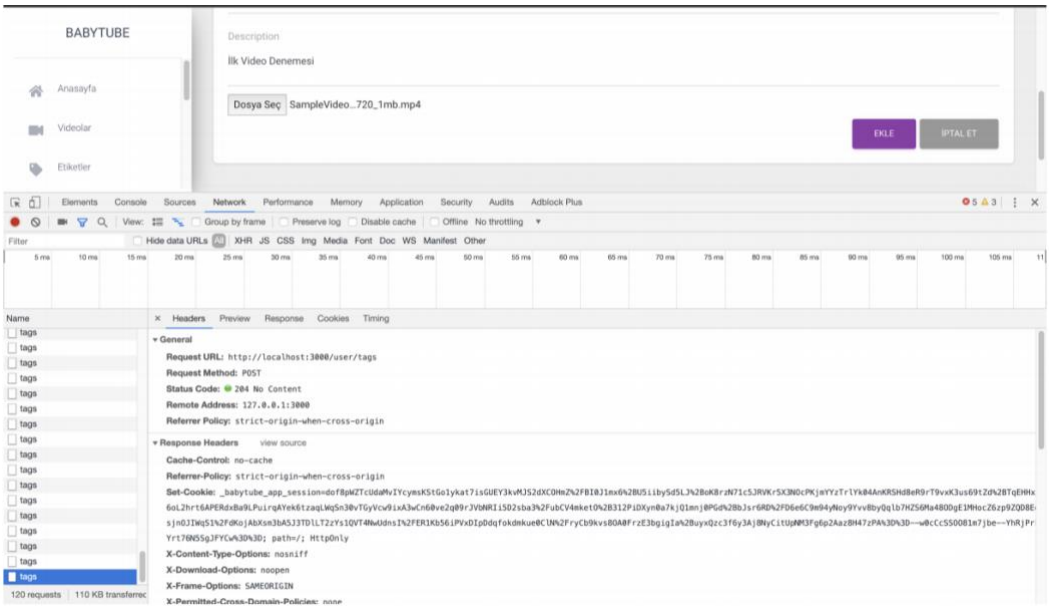

Figure 9. The analysed tags are sent to be saved in the Tag table with POST request.

If a video with a forbidden word tag is tried to be uploaded to the system, a message like this " The video cannot be added to the database." is generated. Thus, as a result of the analysed video, it is checked whether there is a blocked tag in the returned tags, and then the video is not recorded. Checking the database shows that the video is not recorded.

After upload video to the Babytube application besides of the blocked tags also can make CRUD operations. Recorded video can be edited and re-analysed when needed can be done. In addition, with this application, the video can be analysed by entering the 'video_id' information of the Youtube video, as well as new videos suitable for the content to be associated with the 'video_id' information can be presented to the user.

In the Figure 11 you can see a sample Youtube video to copy video_id from URL. Figure 12 shows how Youtube 'video_id' is entered into the system. After the 'video_id' is transferred to the system, the tags of the video are generated. Figure 13 shows how the tags obtained from video analysis with Clarifai application appear in the system. In addition, the tags produced for the sample videos presented in Figure 13 and the accuracy values of these tags are listed in Table 2 and Table 3.

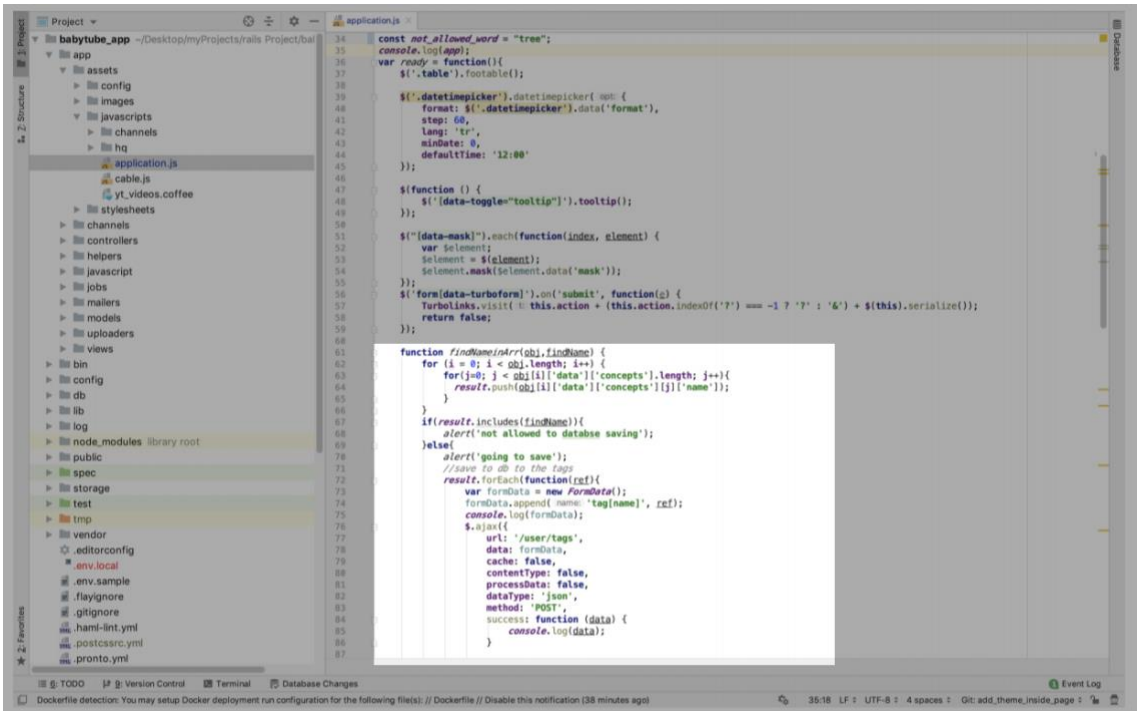

Figure 10. Blocked tags code structure.

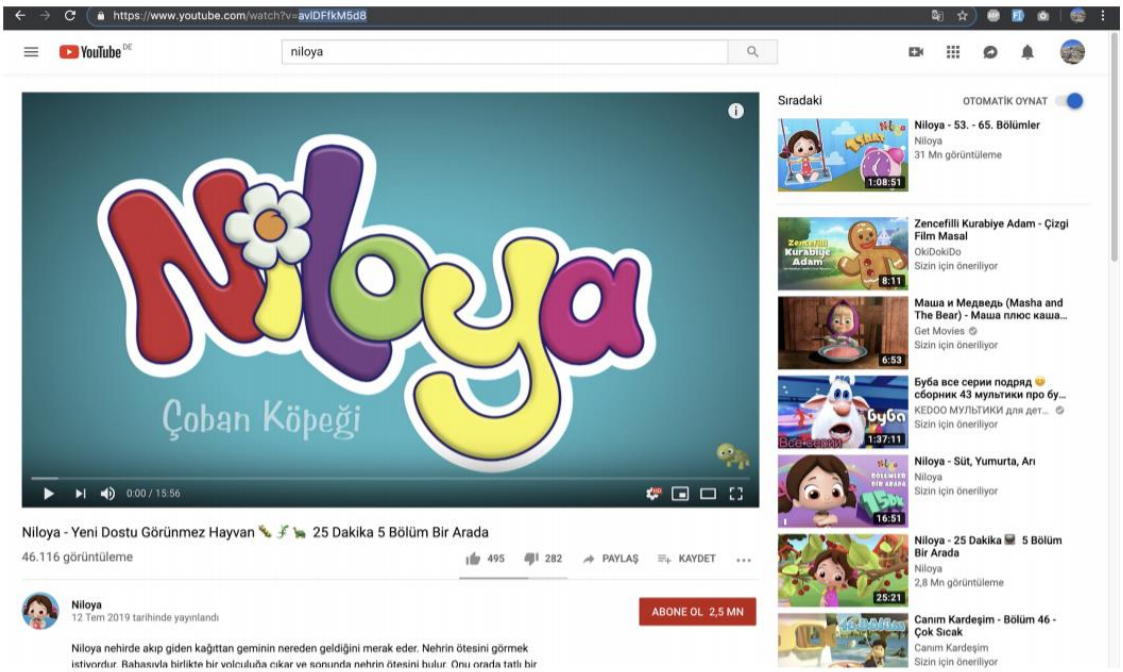

Figure 11. Sample Youtube video and video_id taking process.

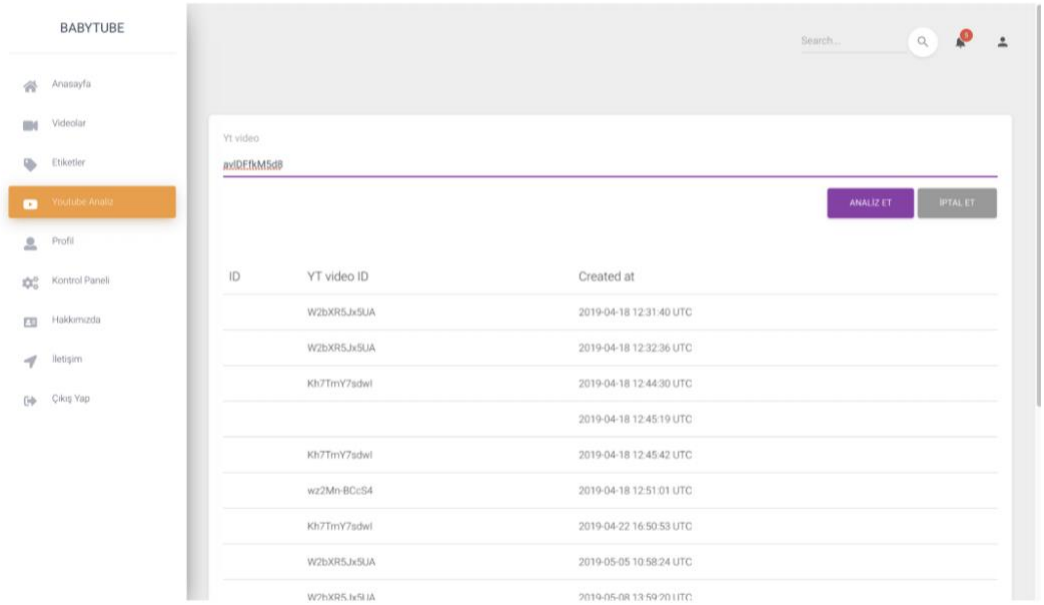

Figure 12. The process of copying Youtube video_id to the system.

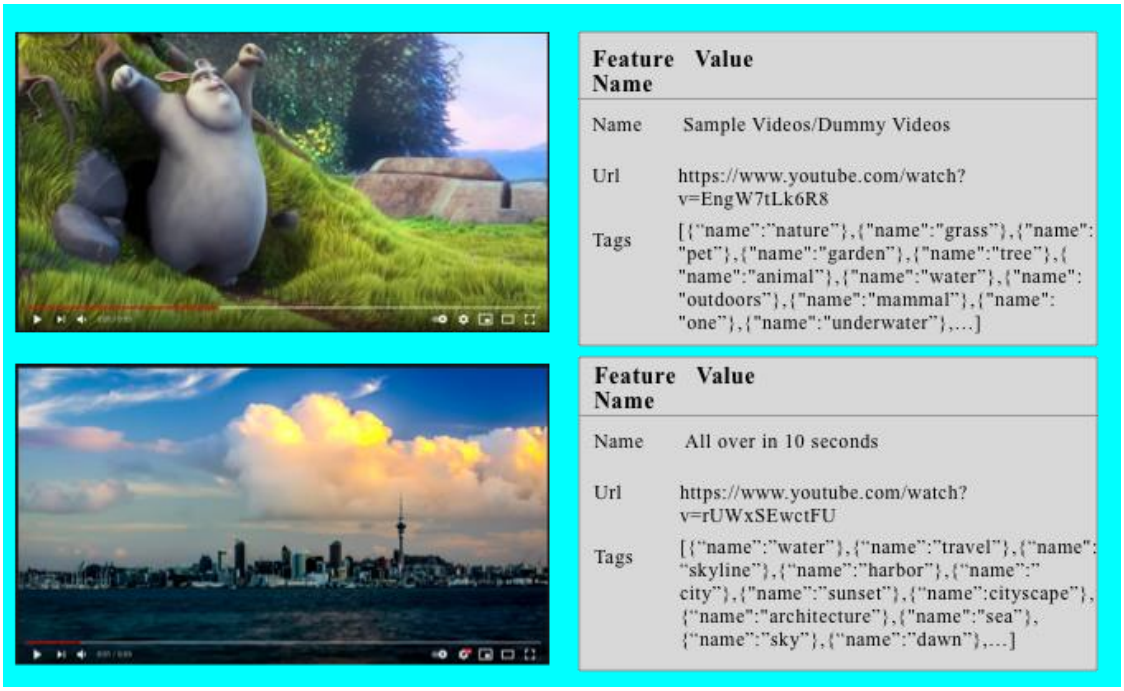

Figure 13. Produced tags of sample Youtube videos.

The analysis of sample videos was completed in an average of 2.32 seconds. The analysis size of the tags is 2.4 KB. In Hamburg, Germany location, the connection speed for video analysis: PING, 7 ms, download speed: 47.94 Mbps, upload speed: 21.95 Mbps. When these values are evaluated in terms of both accuracy and speed, they clearly reveal the power of the system. According to the results of video/image analysis, not only objects but also emotions and qualities can be detected in the system. In this paper, which was done by combining the power of Ruby and Clarifai, when the bad results were removed, an accuracy rate of more than 90% was obtained. The results showed how compatible, healthy, and efficient Ruby, Ruby on Rails and Clarifai technologies work together. The system, which is being developed, will be able to produce more complex images and high accuracy results from different angles of view over time.

Table 2. The generated tags of sample video 1 with value > = 86

Tag	Value	Tag	Value
No person	0.98213712	One	0.92060080
Nature	0.97338900	Underwater	0.92057510
Grass	0.96640030	Daylight	0.90931606
Pet	0.95263130	Cat	0.90702266
Garden	0.95035094	Zoo	0.90313100
Tree	0.94993630	Wildlife	0.89472330
Animal	0.94633630	Invertebrate	0.89044440
Water	0.94495314	Travel	0.86799794
Outdoors	0.94276816	Landscape	0.86431860
Mammal	0.92714000	Fish	0.86011720

Table 3. The generated tags of sample video 2 with value > = 87

Tag	Value	Tag	Value
Water	0.99300100	Dawn	0.96019346
City	0.98977834	Building	0.95924324
Sunset	0.98438900	Downtown	0.95898900
Travel	0.98221534	Pier	0.93812925
Cityscape	0.97174100	Skyscraper	0.91940820
Skyline	0.97047790	Ocean	0.91559740
Architecture	0.96983970	Urban	0.89735160
Harbor	0.96943890	Dusk	0.88911676
Sea	0.96850430	Watercraft	0.88071500
Sky	0.96412070	Port	0.87772230

4. RESULTS AND RECOMMENDATIONS FOR FUTURE STUDIES

In this study, a Ruby on Rails based application has been developed to make technological device and internet usage of children safer and healthier. This developed software automatically tags the contents in the web environment with Ruby on Rails based video and image processing. Using automatic content tagging, personal content control can be performed by providing systematic control over the web 7/24. It is thought that this approach will contribute to strengthening the social communication of people in the early childhood and developing their imaginations. The accuracy of the Ruby on Rails based video and image processing application has been tested with various machine learning techniques in this study. Therefore, it can be said that the developed software will pave the way for children to be mentally, physically and sensually healthier. The improvable parts of the BabyTube application can be listed as follows:

- With an integration to be added to the application, Youtube videos can be analyzed systematically.
- Authorization can be given to pedagogues to interact.
- The "Disorders" part, which is present in the infrastructure but not visible at the interface, can be detailed and the video ranking can be done according to this menu.
- Different analyzes can be made with the generated labels and their graphical representation can be provided
- A timer for children's screen usage can be added.
- Using Metrica, features such as user mood, disorder detection can be added as a result of the analysis of mouse movements.

5. ACKNOWLEDGEMENTS

Abstract version of this paper was presented at International IDU Engineering Symposium – IES'20, December 5-6 and 10-13, 2020, Izmir, Turkey with the title of "Ruby on Rails Based Automatic Video and Image Tagging Application".

6. REFERENCES

1. Akgündüz, D., & Akpınar, B. C. (2018). Okul Öncesi Eğitiminde Fen Eğitimi Temelinde Gerçekleçtirilen STEM Uygulamalarının Öğrenci, Öğretmen ve Veli Açısından Değerlendirilmesi.

2. Aral, N., & Doğan Keskin, A. (2018). Ebeveyn bakış açısıyla 0-6 yaş döneminde teknolojik alet kullanımının incelenmesi. Addicta: *The Turkish Journal on Addictions*, 5(2), 317-348.

3. Bächle, M., & Kirchberg, P. (2007). Ruby on rails. *IEEE software*, 24(6), 105-108.

4. Claxton, G., Rae, M., Long, M., Damico, A., Whitmore, H., & Foster, G. (2016). Health benefits in 2016: family premiums rose modestly, and offer rates remained stable. *Health Affairs*, 35(10), 1908-1917.

5. Clarifai, Technology, (2021). Available at: https://www.clarifai.com/technology (retrieved March 13, 2021).

6. Çevik, G., Yilmaz, R. M., Goktas, Y., & Gülcü, A. (2017). Okul Öncesi Dönemde Artirilmiş Gerçeklikle Ingilizce Öğrenme. *Öğretim Teknolojileri Ve Öğretmen Eğitimi Dergisi*, 6(2), 50-57.

7. Dilekmen, M., & Bozan, N. (2014). Okul Öncesi Eğitimde Oyunun Öğretmen Görüşlerine Göre Değerlendirilmesi. *Atatürk Üniversitesi Kazım Karabekir Eğitim Fakültesi Dergisi*, (37), 43-56.

8. Ergüney, M. (2017). İnternetin Okul Öncesi Dönemdeki Çocuklar Üzerindeki Etkileri Hakkında Bir Araştırma. *Ulakbilge Sosyal Bilimler Dergisi*, 5(17), 1917-1938.

9. Güngör, M. (2014). Okulöncesi Dönem Çocuklarının Televizyon İzleme Alışkanlıkları Ve Anne Baba Tutumları. *Mustafa Kemal Üniversitesi Sosyal Bilimler Enstitüsü Dergisi*, 11(28), 199-216.

10. Flanagan, D., & Matsumoto, Y. (2008). The Ruby Programming Language: Everything You Need to Know. " O'Reilly Media, Inc.".

11. Kacar, A. Ö., & Doğan, N. (2007). Okul öncesi eğitimde bilgisayar destekli eğitimin rolü. *Akademik Bilişim*, 31, 1-11.

12. Kanishcheva, O., & Sharonova, N. (2018). Image and Video Tag Aggregation. *In AIST* (pp. 161-172).

13. Kapi, L. (2019). Erken çocukluk dönemi gelişimi için ruby on raıls temellı vıdeo ve resım işleme uygulaması: Babytube (Master's thesis, Pamukkale Üniversitesi Fen Bilimleri Enstitüsü).

14. Li, X., Xu, C., Wang, X., Lan, W., Jia, Z., Yang, G., & Xu, J. (2019). COCO-CN for cross-lingual image tagging, captioning, and retrieval. *IEEE Transactions on Multimedia*, 21(9), 2347-2360.

15. Ruby on Rails Software, (2021). Avaliable at: https://rubyonrails.org/ (retrieved March 13, 2021).

16. Sayan, H. (2016). Okul Öncesi Eğitimde Teknoloji Kullanımı. *21. Yüzyılda Eğitim Ve Toplum Eğitim Bilimleri Ve Sosyal Araştırmalar Dergisi*, 5(13).

17. Şahin, M. K., & Akman, B. (2018). Erken Çocukluk Döneminde Düşünme Becerilerinin Gelişimi. *Milli Eğitim Dergisi*, 47(218), 5-20.

DOI: 10.38061/idunas.843533

IDUNAS | NATURAL & APPLIED SCIENCES JOURNAL | 2021 Vol. 4 No. 2 (53-60)

Static Compression and Dynamic Sliding Conditions of 2D Trapezoid Square and Circle Contact Surface Shapes

Research Article

Mustafa Murat Yavuz[1*]

[1]Department of Mechanical Engineering, İzmir Democracy University, İzmir, Turkey.

Author E-mails
murat.yavuz@idu.edu.tr
*Correspondance to: Mustafa Murat Yavuz, Department of Mechanical Engineering, İzmir Democracy University, İzmir, Turkey.
DOI: 10.38061/idunas.843533

Received: 19.12.2020; Accepted: 17.02.2021

Abstract

In addition to the commonly encountered force-body interaction problems, deformable body problems are frequently encountered in engineering applications and examination conditions are more complex. The friction force and contact pressure formed between the surfaces have dominant effects and mostly studies are investigated considering static and quasi-static conditions. However, considering the elastic/elasto-plastic deformation and dynamic conditions, the geometric surface shape is important. In this study, using the finite element analysis method, the pressure distribution of the surfaces containing square, trapezoidal and circular surface shapes on a flat surface and the dynamic deceleration condition during the surface interaction of an object with initial velocity are investigated. The material used is steel whose ground geometry does not show linear behaviour and nylon material is used for surface geometry. In order to ensure that the surface effect is dominant in the dynamic examination, a linear increasing pressure is applied on the examined part. In the results, it was determined that there was an irregularity in the stress and velocity deceleration curve. The effect of compression pressure and friction coefficient has been examined in detail and the results are discussed.
Keywords: Contact pressure, surface stress, dynamic, deformation.

1. INTRODUCTION

The deformation of the contact surfaces due to mechanical effects is an important factor for the parts. The effects on the contact surfaces vary depending on the applied pressure and the friction force between the surfaces. However, surface shapes are also important because deformation in dynamic conditions changes the contact surfaces and shape significantly. The flat contact surface is designed differently according to the conditions. Haines and Ollerton [1] studied contact stress distributions on elliptical contact surfaces considering Hertz theory. The adhesive effects caused different shear stress distribution rather than simple strip theory. Johnson et al. [2] discussed the force of adhesion and contact size effect between two spherical solid surfaces. Surface energy concept was considered with rubber and gelatine spheres. In literature, contact surface shapes [3] were optimized for better and more uniform contact

pressure distribution. Senouci et al. [4] investigated wear behaviour of graphite-copper sliding contact. Anisotropic graphite causes incompatibility between mechanical and tribological behaviour. Kimura et al. [5] investigated wear and fatigue of contact rollers in which microslip condition had a dominant effect. Herskovits et al. [6] prepared a bilevel program for shape optimization of elastic solids contact problems. Both shape optimization and nonlinear contact analysis solutions were carried out simultaneously. Li et al. [7] studied on shape optimization for contact problems including combined loadings. Goryacheva et al. [8] considered partial slip conditions in fretting and prepared an analytical model. Archard's wear law was used for wear development and they calculated contact pressure and shear stress, contact width, gap and slip functions using stepwise formulation. Brake pads including hatched shapes [9] were considered that increases fade resistance. Araujo and Nowell [10] investigated effect of contact stress variation on fretting fatigue and demonstrated contact size effect in fretting fatigue life. Triangle, trapezoid, parallelogram and rectangular block shapes [11] were investigated for stress reduction in tilt tests. Jiang et al. [12] studied 3D elasto-plastic stress analysis of contact rollers with kinematic hardening. Shear tractions had a dominant effect on residual stresses and strains. Wen et al. [13] modelled wheel/rail contact-impact behaviour with kinematic hardening. During dynamic analysis, peak force effect was observed 2.6 times greater than static results. Gerlici and Lack [14] investigated influence of contact geometry and calculated surface stress distributions of wheel-rail interaction. Rovira et al. [15] and Dirks and Enblom [16] studied on contact and wear interaction of wheel-rail. Contact interface of adhesive binding [17] was investigated for optimal surface shapes. Contact behaviour of complex surface shapes [18] were investigated for punches.

In this study, using the finite element method, contact levels with different surface shapes in dynamic conditions have been investigated. The study is made in 2D. Properties of different compression pressures were used, and the effect of the friction coefficient was examined separately. Results are compared as Von-Mises stress.

2. MODELS AND METHOD

Three different surface shapes used in the study were shown in Fig. 1. Surface shapes formed in trapezoid, circular and rectangular shapes were studied on a flat plane with the initial velocity in the horizontal right direction. Initial velocity is 5 m/s horizontally. All geometric properties in 2D are shown in the Fig. 1. Different shaped parts contacting the surface as material are selected as nylon and other parts are modelled to include steel material properties. While the moving contact surface modelled in different geometries contains nylon properties, other parts are modelled to contain steel material properties. 0.1 MPa surface pressure applied to the shoe geometry to see the friction effect more clearly. Solution time was chosen as 1.4 milliseconds (ms).. Friction coefficient is used as 0.3 as default. Fancelle et al. [19] used Augmented-Lagrangian algorithm for contact modelling and interior-point method for shape optimization in 2D frictionless finite element solution. Similarly, Augmented-Lagrange contact algorithm was used in this analysis.

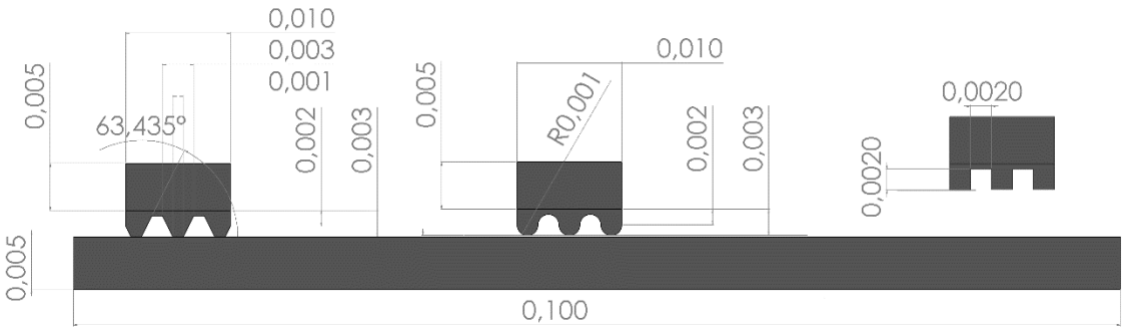

Figure 1. Models of trapezoid, circle and square contact surface shapes.

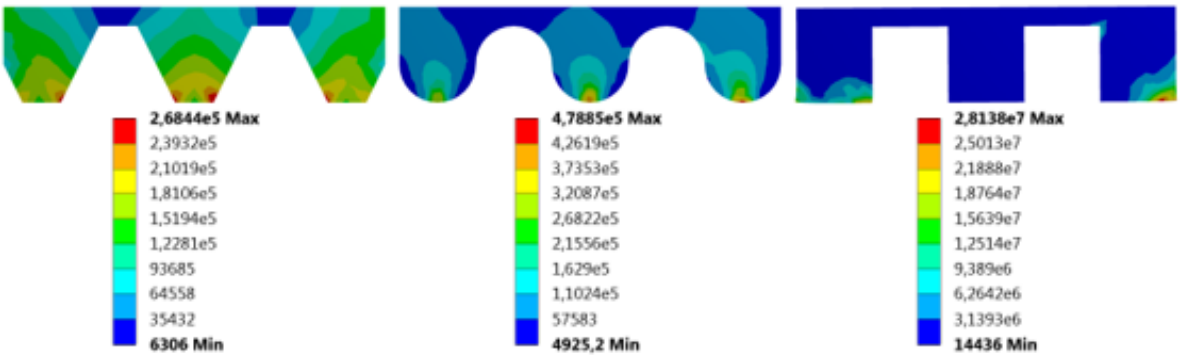

Figure 2. Von-Mises stresses of trapezoid, circle and square contact surface shapes.

The Von-Mises stresses created by different contact geometries were shown in Fig. 2. Considering the results, the stress density formed at the end corners of the trapezoid geometry. The intensity of this stress was mostly at the inner corners of the 3 pieces. In the round tip contact geometry, the stress distribution occurred as a result of full contact. In the rounded contact geometry, the stress distribution occurred at the full contact end points. The stress value was approximately 2.6 times higher than applied pressure which was similar results of the Wen et al. [13] study Considering the stress results in the square shaped model, it was seen that the stress reached the highest value at the corner end in the direction of movement and a stress jump was determined. The low stress in the square geometry in the middle section indicated a non-contact condition. At this point the stress value was 100 times higher than the results of the trapezoid shape. Fig. 3 results showed the coefficient of friction results for round geometries. Stress distributions were formed in the same structure with different friction coefficients. However, with the increasing friction coefficient, the stress values first decreased and then remained constant. Fig. 4 results showed the effect of applied contact pressure. Considering the results, increasing the applied contact pressure allowed to increase stress values to very high. In the last case, the stress value remained approximately the same.

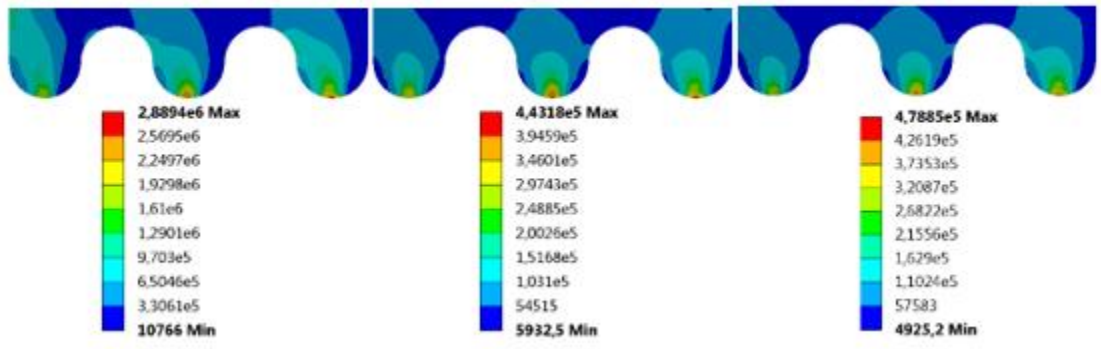

Figure 3. Von-Mises stresses of circle contact surface shape under 0.2, 0.25, 0.3 friction coefficient.

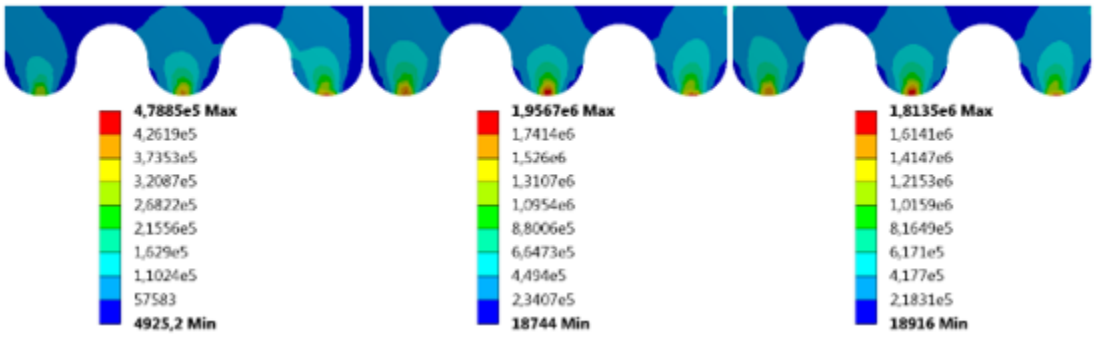

Figure 4. Von-Mises stresses of circle contact surface shape under 0.1, 0.2 and 0.3 MPa compression pressure.

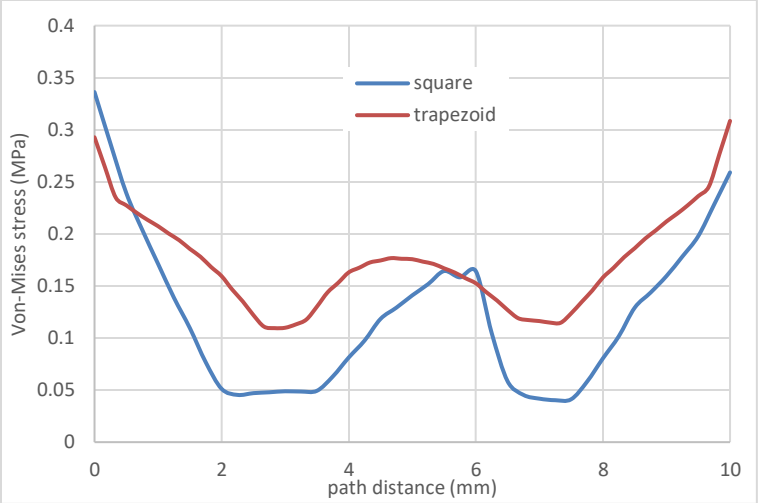

Figure 5. Von-Mises stresses of square and trapezoid contact surface shape under static compression.

In Fig. 5, the stress distribution on the line 1 of the body with square and rectangular contact surfaces was shown in the graph. As a result of the examination, the stresses were higher at the corner ends, at the middle level in the middle and at the lowest level in the partition lines. The shape consists of 3 parts and the structure of the space between them caused this distribution.

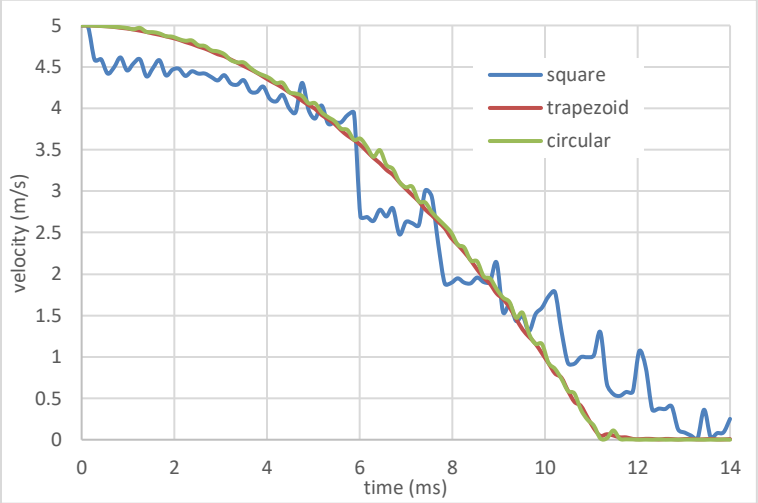

Figure 6. Velocity of trapezoid, circle and square contact surface shapes under time.

In Fig. 6, the deceleration graph of the contact surfaces with different geometric structures according to time was shown. All parts stopped at the time of 14 ms. This solution was implemented for 0.1 MPa and 0.3 friction coefficient. While the trapezoid and circular cross-section exhibited the same smooth profile, the square geometry had a very wavy structure. The non-contact situation was available in the square geometry solution. In Fig. 7, the effect of different friction coefficients was shown. In the solution using circular cross section and 0.1 MPa, a faster deceleration was achieved as a result of the increased friction coefficient. In the solution where the friction coefficient was 0.2, the part, which can stop in 14 ms, could stop in 11.6 ms when the coefficient was increased to 0.3.

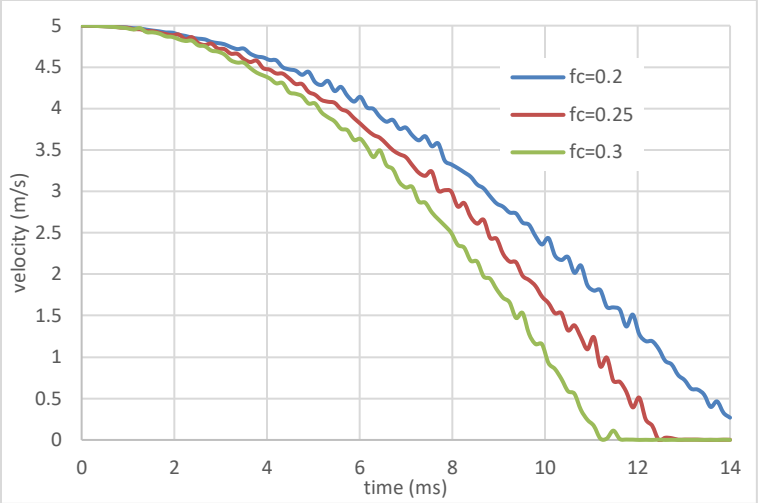

Figure 7. Velocity of circle contact surface shape under 0.2, 0.25, 0.3 friction coefficient under time.

In Fig. 8, the applied contact pressure effect was shown for the deceleration case. Stopping occurred at 11.6 ms at 0.1 MPa applied contact pressure, while at 0.2 MPa in 8 ms and at 0.3 MPa in 6.5 ms. In Fig. 9, the stress plot of all brake surfaces versus time was given. Accordingly, the square geometry used exhibited a very high stress profile. The irregular distribution was due to the regional interruption of the contact over time. Contact was maintained in the circle and trapezoid section, and the braking effect was dominant between 9 ms and 11 ms.

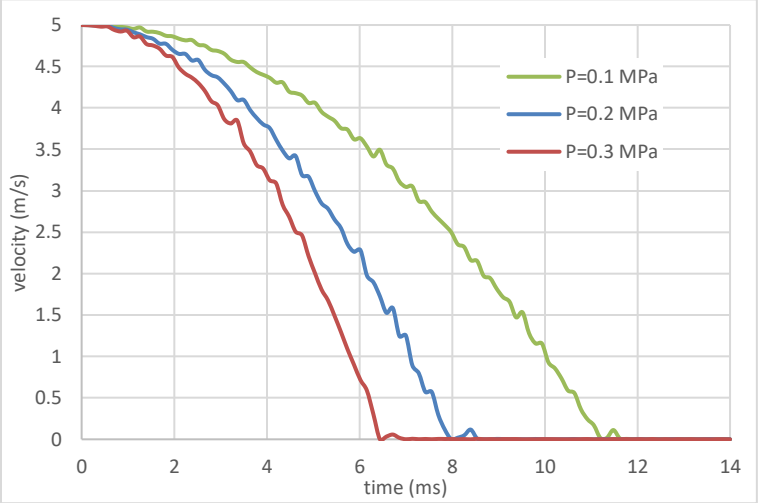

Figure 8. Velocity of circle contact surface shape under 0.1, 0.2 and 0.3 MPa compression pressure under time.

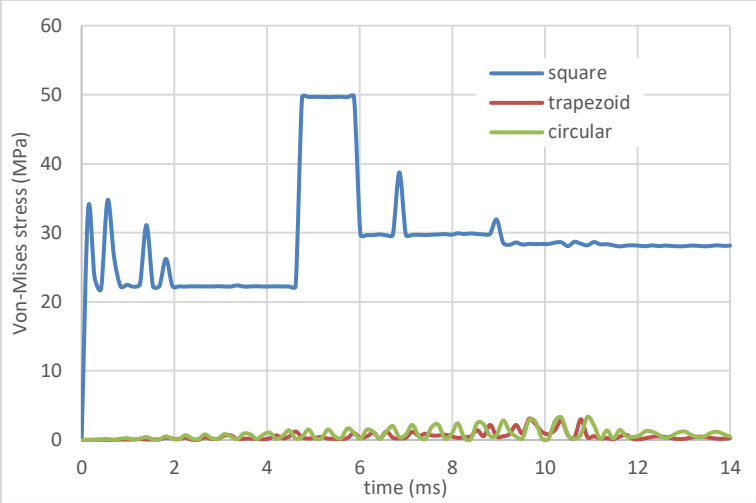

Figure 9. Von-Mises stresses of trapezoid, circle and square contact surface shapes under time

The friction coefficient effect was shown in Fig. 10 for point 1. The wave distribution that was formed as a result of dynamic effects occurred at an amplitude that increases up to 11.5 ms, which was the stopping time of objects. The highest stress amplitude appeared to be within the 0.25 friction coefficient. An instantaneous stress drop was observed in 11.5 ms at 0.2 friction coefficient, but the amplitude continued at high levels in later times. This was the case for the object did not stand still. The applied contact pressure effect was shown in Fig. 11. With the increase in pressure, the increase in amplitude showed a proportional increase. The amplitude of 0.3 MPa decreased in 6.5 ms, as it enabled the objects to stop in a shorter time with increasing contact pressure. The same has been true for other pressure results. A lower stretch amplitude continued after the decrease in amplitude.

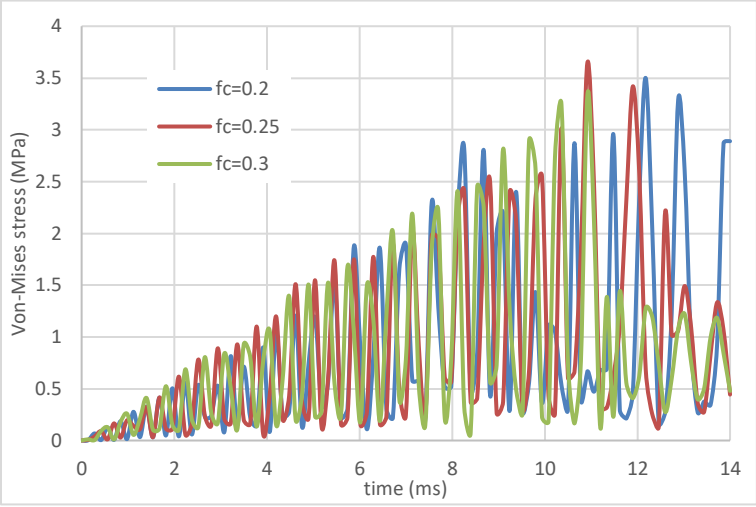

Figure 10. Von-Mises stresses of circle contact surface shape under 0.2, 0.25, 0.3 friction coefficient under time

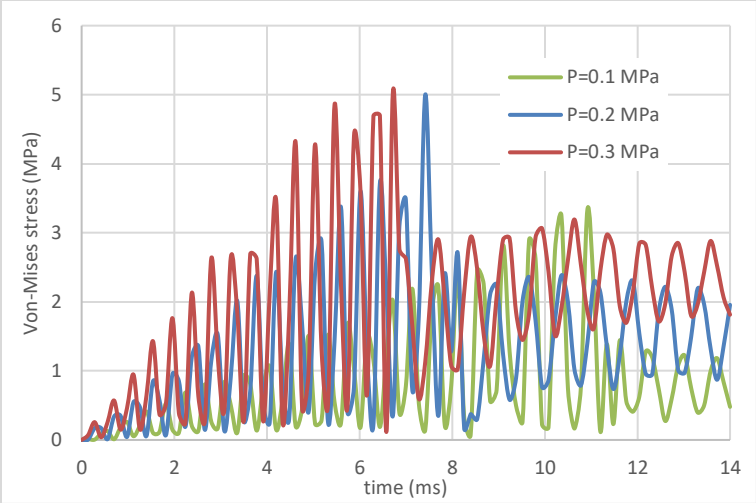

Figure 11. Von-Mises stresses of circle contact surface shape under 0.1, 0.2 and 0.3 MPa compression pressure under time

3. CONCLUSION

Trapezoid, square and circle contact surface shapes are considered for static compression and dynamic sliding conditions. A default 2D case study is applied with 0.1 MPa braking pressure, 0.3 friction coefficient and 5 m/s initial velocity. The friction coefficient and braking pressure was changed. It was observed that;

- Inner corners of trapezoid shape have the highest stress locations, but they are formed at contact points in rounded (circular) shape.
- A non-contact condition was observed in square shape.
- The increased friction coefficient causes to decrease stress values at first than causes to remain constant.
- A non-linear stress increment has been observed when increasing the applied contact pressure.

4. REFERENCES

1. Haines, D.J., and Ollerton, E. (1963). Contact stress distributions of elliptical contact surfaces subjected to radial and tangential forces. Proc Instn Mech Engrs, 177(4).

2. Johnson, K.L., Kendall, K., Roberts, A.D. (1971). Surface energy and the contact of elastic. Proc. R. Soc. Lond. A., 324, 301-313.

3. Páczelt, I., Mróz, Z. (2005). On optimal contact shapes generated by wear, Numerical Methods in Engineering, 63(9), 1250-1287.

4. Senouci, A., Frene, J., Zaidi, H. (1999). Wear mechanism in graphite–copper electrical sliding contact. Wear, 225–229, 949–953.

5. Kimura, Y., Sekizawa, M., Nitanai, A. (2002). Wear and fatigue in rolling contact. Wear, 253, 9–16.

6. Herskovits, J., Leontiev, A., Dias, G., Santos, G. (2000). Contact shape optimization: a bilevel programming approach. Struct Multidisc Optim, 20, 214–221.

7. Li, W., Li, Q., Steven, G.P., Xie, Y.M. (2005). An evolutionary shape optimization for elastic contact problems subject to multiple load cases. Comput. Methods Appl. Mech. Engrg., 194, 3394–3415.

8. Goryacheva, I.G., Rajeev, P.T., Farris, T.N. (2001). Wear in partial slip contact. Transactions of the ASME, 123, 848-856.

9. Albatlan, S. A. A. (2013). Study effect of pads shapes on temperature distribution for disc brake contact surface. International Journal of Engineering Research and Development, 8(9), 62-67.

10. Araujo, J.A., Nowell, D. (2002). The effect of rapidly varying contact stress fields on fretting fatigue. International Journal of Fatigue, 24, 763–775.

11. Kim, D. H.; Gratchev, I. Hein, M. Balasubramaniam, A. (2016). The application of normal stress reduction function in tilt tests for different block shapes. Rock Mechanics and Rock Engineering, 49, 3041–3054.

12. Jiang, Y., Xu, B., Sehitoglu, H. (2002). Three-dimensional elastic-plastic stress analysis of rolling contact. Journal of Tribology, 124, 699-708.

13. Wen, Z., Jin, X., Zhang, W. (2005). Contact-impact stress analysis of rail joint region using the dynamic finite element method. Wear, 258, 1301–1309.

14. Gerlici, J., Lack, T. (2010). Contact geometry influence on the rail / wheel surface stress distribution. Procedia Engineering, 2, 2249-2257.

15. Rovira, A., Roda, A., Marshall, M.B., Brunskill, H., Lewis, R. (2011). Experimental and numerical modelling of wheel–rail contact and wear. Wear, 271, 911– 924.

16. Dirks, B., Enblom, R. (2011). Prediction model for wheel profile wear and rolling contact fatigue. Wear, 271, 210–217.

17. Yao, H. Gao, H. (2016). Optimal shapes for adhesive binding between two elastic bodies. Journal of Colloid and Interface Science, 298(2), 564-572.

18. Kazakov, K. E. (2018). Contact between a regular system of punches and a layered foundation with consideration of complex surface shapes. AIP Conference Proceedings, 2053(1), 040041.

19. Fancelle, E.A., Haslinger, J., Feijoo, R.A. (1995). Numerical comparison between two cost functions in contact shape optimization. Structural Optimization 9, 57-68.